

MENSA: A Multi-Event Network for Survival Analysis with Trajectory-based Likelihood Estimation

Christian Marius Lillelund

CLILLELUND@UALBERTA.CA

Dept. of Computing Science, University of Alberta, Canada

Dept. of Elec. and Comp. Engineering, Aarhus University, Denmark

Ali Hossein Gharari Foomani

HOSSEING@UALBERTA.CA

Weijie Sun

WEIJIE2@UALBERTA.CA

Shi-ang Qi

SHIANG@UALBERTA.CA

Dept. of Computing Science, University of Alberta, Canada

Russell Greiner

RGREINER@UALBERTA.CA

Dept. of Computing Science, University of Alberta, Canada

Alberta Machine Intelligence Institute, Canada

**The Pooled Resource Open-Access ALS
Clinical Trials Consortium (PRO-ACT)[†]**

Abstract

A multi-event survival model predicts the time until an instance experiences each of several different events, given the instance’s description. Unlike competing-event models, the events here are not mutually exclusive and often exhibit statistical dependencies. Existing approaches for multi-event survival analysis have generally been limited, most focusing on producing simple risk scores for each event, rather than the time-to-event itself. To overcome these issues, we introduce MENSA, a novel deep learning approach for multi-event survival analysis. MENSA jointly learns representations of the input features while capturing the complex dependence structure among events. In practice, it attempts to optimize the sum of the traditional negative log-likelihood across events and a novel trajectory-based likelihood, which encourages the model to learn the temporal order in which events occur. Experiments on real-world clinical datasets show that MENSA consistently gives good discrimination performances and accurate time-to-event predictions in single-event, competing-risk, and multi-event problems. Additionally, MENSA is more computationally-efficient, requiring fewer parameters and FLOPs than multiple state-of-the-art survival baselines when applied to large-dimensional datasets (more than 100 features).

Keywords: Machine learning, survival analysis, competing risks, multi-event, precision medicine

1 Introduction

Many survival analysis models estimate the probability that some specific event (typically death) will occur for an individual at time T later than t , for all times $t > 0$ (Gareth et al., 2021, Ch. 11). Learning such models is challenging for standard regression tasks, as the training dataset can include many censored instances – cases where we only have a lower bound on the actual time of the occurrence. This problem can be extended to deal with many possible events – such as death from cancer, and also death from heart failure. This can involve *competing risks*, where the occurrence of one event excludes the others

(*e.g.*, one can either die from cancer or from heart failure, but not both) or *multi-event* scenarios, where the occurrence of one event does not exclude the others, such as different types of medical emergencies in hospitalized patients, *e.g.*, acute respiratory failure (ARF) or shock (Tjandra et al., 2021), or adverse effects in patients who underwent a bone marrow transplantation, *e.g.*, relapse or death (Marta Fiocco, 2008).

As a practical example, consider a drug trial over $t \in [0, 100]$ days, where some patient i (*e.g.*, Mr. Smith) with some description $\mathbf{x}^{(i)}$ can experience 4 side effects: nausea (A), fatigue (B), fever (C) or headache (D). In survival analysis, we want to predict the survival probability (*i.e.*, the probability that the event occurs at T later than some time t) for each of these possible side effects over a finite time horizon, *e.g.*, from 0 to 100 days. We can address this problem as a multi-event survival problem and build a single model to estimate the so-called individual survival distribution (ISD) of each of these four events for Mr. Smith, which we denote as $\hat{S}^{(i)}$ (see Figure 1). Thus, these ISDs give the probability of each of these 4 events occurring after t days post-baseline, for all $t > 0$. We can also use these ISDs to estimate the probable time-to-event for Mr. Smith, for example, when the survival (event) curve intersects the dashed horizontal line at 50%, for each of the events.

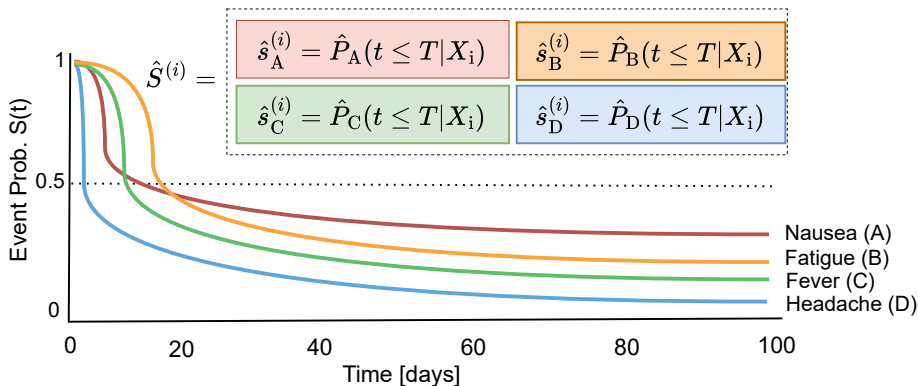


Figure 1: Outline of a multi-event survival prediction with four events.

In the current literature, some practitioners - *e.g.*, Armstrong et al. (2014); Solomon et al. (2017) - simply use many single-event models for these multi-event problems. Perhaps one Cox Proportional Hazards (CoxPH) model (Cox, 1972) for cancer, and another for heart failure by modeling each event separately. This approach has multiple issues: (1) Separate models fail to leverage the shared patterns or features (covariates) between different events, however, real-world events often follow temporal or causal patterns that influence or correlate with each other, *e.g.*, illness usually occurs before death (Fix and Neyman, 1951). (2) Training a new model for each event requires significant computational resources, particularly for large datasets or when there are many events of interest. (3) As the number of events increases, it becomes cumbersome to manage multiple single-event models. In contrast, a single multi-event model scales more efficiently by handling all events within a single architecture. There are, however, very few effective multi-event survival models in the literature, and most only deal with risk scores - *i.e.*, simply attempting to identify the order of the events, both for each single individual, and also between individuals. However,

we often need models that provide not only good discriminative performances (Tjandra et al., 2021), but also accurate time-to-event estimates (Qi et al., 2023a).

In this paper, we propose a Multi-Event Network for Survival Analysis (**MENSA**). MENSA is a novel and scalable deep learning model for multi-event survival analysis, that learns the K event distributions jointly, where each event is a convex combination of Weibull distributions. This approach relaxes the proportional hazards assumption about the underlying marginal survival distribution for each event, which is a significant limitation for Cox-based methods (Cox, 1972; Katzman et al., 2018; Lillelund et al., 2024b). As in previous works (Lee et al., 2018; Tjandra et al., 2021), we adopt a shared feature (covariate) layer in our architecture that captures the latent feature representation common to all events. Moreover, beyond simply optimizing the negative log-likelihood (NLL) over all events (Tjandra et al., 2021), we propose optimizing the sum of the NLL and a novel trajectory-based likelihood, which encourages the model to match the known temporal orderings between events based on prior knowledge. For example, consider the illness-death scenario (Fix and Neyman, 1951) with two events “illness (A)” and “death (B)”: If both events are observed for the patient i , then clearly event A must occur before event B, and so we want to maximize the probability of surviving event B, at the time of event A – so if A happened at 1 year, we want the probability of surviving B at 1 year to be very high.

MENSA is inspired by the multi-state framework, originally proposed by Andersen and Keiding (2002), where an event can be considered a transition from one state to another – *e.g.*, alive to dead, or healthy to sick. This framework enables us to model the event-free distribution (*i.e.*, the transient state) explicitly as if it were another event and perform likelihood estimation in conjunction with the events of interest. This allows practitioners to predict whether a patient will remain event-free for the duration of the study, along with other events. In addition, the MENSA framework easily extends to the single-event and competing-risk scenarios, making it suitable for a wide range of applications.

We provide experimental evidence to show that MENSA can accurately discriminate (*i.e.*, rank) instances by risk and make time-to-event predictions that improve over several shallow and deep learning baselines. We show that MENSA strikes a good balance between various evaluation tasks, *e.g.*, discrimination, prediction, and calibration, without sacrificing either. Furthermore, MENSA uses fewer parameters and floating point operations per second (FLOPs) in high-dimensional datasets than many existing neural network approaches. Ablation experiments demonstrate that applying a shared feature layer can improve predictive performances if conditional dependencies exist between events, and that the proposed trajectory likelihood improves the accuracy of the time-to-event estimates.

Our code is publicly available at <https://github.com/thecml/mensa>

2 Related work

Single-event analysis. Time-to-event outcomes have been extensively studied within the field of survival analysis, primarily by the statistical, medical, and reliability engineering communities (Chen, 2024). Traditional single-event models aim to learn the time until a single event occurs for an instance, for example, the time to death in amyotrophic lateral sclerosis (ALS) (Kuan et al., 2023), the time to fall in community-dwelling elderly (Lillelund et al., 2024a), or various other events in economic and social sciences. In practice, “survival

prediction” does not necessarily refer to actual mortality. The challenge in survival prediction is that the event times can be partially observed (*i.e.*, censored), providing only a lower bound on the true event time. Multiple censoring mechanisms may exist in practice, but in this work we will focus on the most common form: *right-censoring*, where we know the event occurs after a certain time, but not exactly when.

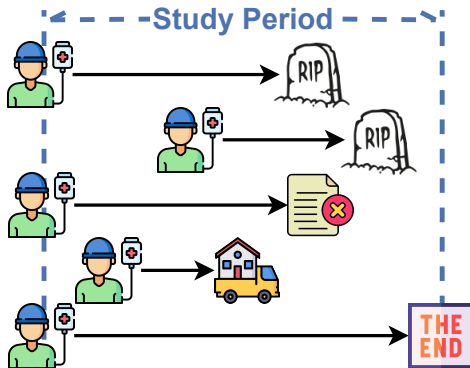


Figure 2: Illustration of right-censorship in survival datasets.

In a medical study as shown in Figure 2, some patients may experience the event (1st and 2nd patient), but some may be lost to follow-up (3rd patient), withdraw from the study (4th patient), or remain alive at the end of the study (5th patient). For these patients, the exact event time is known only to exceed their last contact or the end of the study. A wide range of models have been proposed for this setting, including the nonparametric Kaplan-Meier (KM) (Kaplan and Meier, 1958) and Nelson-Aalen (Nelson, 1969; Aalen, 1978) population estimators, semiparametric proportional hazards models for individuals, *e.g.*, CoxPH (Cox, 1972; Faraggi and Simon, 1995; Katzman et al., 2018), and parametric survival models, *e.g.*, the Weibull time-to-event model (Prentice and Kalbfleisch, 1979), Random Survival Forest (Ishwaran et al., 2008) and Multi-Task Logistic Regression (MTLR) (Yu et al., 2011). Chen (2024) provide an excellent introduction to the field and describe the transition from classical time-to-event methods to modern deep learning approaches.

Competing-risks analysis. In competing-risks survival analysis, there are multiple events of interest, *e.g.*, for a patient, we consider the patient dying from lung cancer, or from pneumonia, as two different events, which are mutually-exclusive. We thus want to learn a model that can predict, for each individual, which event will occur first and the time until this earliest event. Concerning censoring in such scenarios, competing risks is a form of dependent censoring (Emura and Chen, 2018, Ch. 1), as one risk (event) dependently censors the other, and these risks are assumed to have some prior relationship. However, estimating competing-risks data is more challenging than single-event analysis due to the identifiability issue (Tsiatis, 1975); since events are mutually-exclusive, the first event will censor the other events, preventing direct observation of their dependence structure. Given these challenges, multiple methods have been proposed for competing-risks scenarios, usually assuming that events are conditionally independent given the features.

Lee et al. (2018) proposed DeepHit, a discrete-time neural network of the form $f_\theta : \mathbf{x} \rightarrow [0, 1]^{T_{\max} \times K}$ with parameter θ , number of events K , and some maximum observed time T_{\max} . DeepHit contains a shared covariate layer and K cause-specific sub-networks; its learning process learns θ by maximizing the log-likelihood of the joint distribution of K competing events and a cause-specific ranking loss.

Kim et al. (2021) proposed MTLR-CR, an extension of the discrete MTLR framework for competing risks. MTLR (Yu et al., 2011) is a neural network implementation of a discrete-time survival model that predicts the survival distribution using a sequence of dependent logistic regressors. This is then extended to competing-risks scenarios by learning sequences of logistic regressors for the number of discrete time times, for every K event.

Nagpal et al. (2021) proposed Deep Survival Machines (DSM), a parametric survival model based on a mixture of predefined primitive distributions, *e.g.*, a mixture of Weibulls. DSM first learns a common feature representation of all competing risks, and then a k th-event distribution for each event using cause-specific maximum likelihood estimation (MLE), treating all events other than k as censored. However, this approach does not explicitly model the density or survival function relationships between events on a one-to-one basis. As a result, it may not account for potential interdependencies between events.

Multi-event analysis. In multi-event analysis, we again consider multiple critical events, but these are not necessarily mutually-exclusive, as a patient may experience none, one or any subset of events at different times. For example, Mr. Smith may experience the onset of lung cancer at 1 year and may also experience the onset of pneumonia at 1.3 years, meaning that he would have both events (onset of lung cancer and of pneumonia). Multi-event analysis goes back as early as 1951, when Fix and Neyman (1951) introduced the illness-death model, which has been used in multiple subsequent works (Sverdrup, 1965). Unlike competing-risks, multi-event analysis does not necessarily suffer from the identifiability issue (Tsiatis, 1975), as the events are not necessarily mutually-exclusive. However, predicting the outcome of several (possibly related) events instead of just one poses another challenge: When events are, in fact, competing, naive survival models that do not account for the dependency structure between events may produce biased estimates.

Larson (1984) adopted the popular CoxPH model (Cox, 1972) for multi-event survival analysis by modeling each event separately – an idea that has gained popularity since then (Armstrong et al., 2014; Solomon et al., 2017), but which fails to capture any dependencies between the events. Andersen and Keiding (2002) proposed a multi-state model that learns a model for each event transition (*e.g.*, given a person is diagnosed with lung cancer, it then predicts the probability of pneumonia), but this also fails to leverage shared covariate information among the events. Several works have addressed this restriction, *e.g.*, using a shared frailty term across models (Jiang and Haneuse, 2017), applying forms of regularization (Li et al., 2016; Wang et al., 2017) or by modeling the joint survival distribution (Hsieh and Wang, 2018). However, these approaches require assumptions on the distribution of the frailty term, the proportional hazards assumption, or assumptions on the form of the joint survival distribution, respectively.

Tjandra et al. (2021) proposed a hierarchical multi-event model that learns the probability of event occurrence at different hierarchical time scales, using coarse predictions to iteratively guide predictions at finer levels – for example, from monthly to daily predictions. Given a complex task over a long time span, the model decomposes this task

into a sequence of simpler tasks that serve as intermediate guides. Thus, the hierarchical framework progressively predicts survival across multiple time granularities, starting with broader intervals (*e.g.*, months) and refining down to finer ones (*e.g.*, weeks, then days). Formally, their model is a multi-task network that takes x as input and outputs \hat{P} , a set of probability distributions for each k event. Event-specific subnetworks, ϕ_k , estimate the probability distribution \hat{p}_k hierarchically. At granularity m , the probability distribution \hat{p}_{km} is constructed from $\psi_{km}(\Phi(x))$ and the previous granularity level $\hat{p}_{k,m-1}$, ensuring that predictions at finer time scales are guided by coarser ones. However, there are two primary limitations to this approach: (1) the hierarchical component scales poorly with larger time durations and has a significant parametric overhead. (2) the method is optimized solely for discriminative loss — *i.e.*, ranking using Harrell’s concordance index (CI) (Harrell Jr. et al., 1982). However, strong ranking performance does not necessarily translate into accurate time-to-event predictions (Qi et al., 2023a), and vice versa. In our experiments, we will highlight these two limitations to the hierarchical model, *i.e.*, its computational overhead and lack of predictive accuracy. Lastly, in Tjandra et al. (2021), the model is not evaluated on any real-world, multi-event dataset, but only on synthetic data. This can be problematic because synthetic datasets may not capture the complexity, variability, and noise present in real-world data.

3 Fundamentals

3.1 Survival data and notation

Survival analysis, or time-to-event prediction, models the time until an event of interest takes place (Gareth et al., 2021, Ch. 11). We can represent such problems using a two-state model, as depicted in Figure 3a. In this simplest case, there is one transient state (0, *e.g.*, “alive”) and one absorbing state (1, *e.g.*, “dead”) (Andersen and Keiding, 2002). Once an individual enters an absorbing state, no further transitions are possible. The observation for a given instance will in the most simple form consist of a random variable, T , representing the time from a given origin ($t = 0$) to the occurrence of the event, *e.g.*, “death”. The distribution of T can be characterized by the probability distribution function $F(t) = \Pr(T \leq t)$ or, equivalently, by the survival function $S(t) = 1 - F(t) = \Pr(T > t)$. Note that $S(t)$ and $F(t)$, respectively, correspond to the probabilities of being in state 0 or 1 at time t . In our survival analysis framework, we want to estimate the probability that some specific event occurs at time T later than t (for each $t > 0$), *i.e.*, the survival probability, $S(t) = \Pr(t > T) = 1 - F(t)$. In continuous time, the distribution of T can be characterized by the *hazard rate function*:

$$a(t) = -d \log S(t) / dt = \lim_{\Delta t \rightarrow 0} \frac{\Pr(t < T \leq t + \Delta t | T > t)}{\Delta t}, \text{ that is, } S(t) = \exp \left(- \int_0^t a(u) du \right).$$

Here, $a(t)$ is the transition intensity from state 0 to 1, *i.e.*, the instantaneous probability of going from state 0 to state 1 at time t . A defining characteristic of survival analysis is that many of its training instances are censored, where we only have a lower bound on the event time of those instances. This includes, for example, individuals who are still alive at the end of the study, as well as others who left the study and were “lost to follow-up”

– this is known as *right-censoring*. In order to make valid inferences on parameters in a multi-state model based on incomplete data, we often assume *independent* right-censoring, *i.e.*, $T_E \perp\!\!\!\perp T_C$, where $T_E \in \mathbb{R}_+$ is a nonnegative random variable (R.V.) representing the event time, and $T_C \in \mathbb{R}_+$ is the R.V. representing the censor time. This basically means that a sample observed after *independent* right-censoring is representative of the population without censoring, and thus censored individuals have neither lower nor higher risk of future events than uncensored individuals. If features are entered into the model using a regression model for $a(\cdot)$, this restriction is typically relaxed, and it is assumed that the event of interest is *conditionally independent* given the features, *i.e.*, $T_E \perp\!\!\!\perp T_C \mid X$, where $X \in \mathbb{R}^d$ is the R.V.s for features.

In this context, we may define our survival dataset as a set of observations, $(\mathbf{x}^{(i)}, t^{(i)}, \delta^{(i)})$, where $\mathbf{x}^{(i)} \in \mathbb{R}^d$ is a feature vector for instance i , $t^{(i)} \in \mathbb{R}$ is the time of either censoring or event, depending on which occurred first, and $\delta^{(i)} \in \{0, 1\}$ is the ‘‘censoring bit’’: If $\delta^{(i)} = 0$, then $t^{(i)} = c^{(i)}$, where $c^{(i)}$ is the time of censoring, otherwise, if $\delta^{(i)} = 1$, then $t^{(i)} = e^{(i)}$, where $e^{(i)}$ is the time of the event. Given survival data $\mathcal{D} = \{(X^{(i)}, T^{(i)}, \delta^{(i)})\}_{i=1}^N$, let $f_{T_E|X}(\cdot)$ and $F_{T_E|X}(\cdot)$ represent the conditional density and cumulative distribution functions of the event, respectively, over the event horizon $[0, \dots, t_{\max}]$. The likelihood of the i -th instance experiencing the event of interest can then be determined:

$$\mathcal{L}(\mathcal{D}^{(i)}) = \Pr(T_E = t^{(i)}, T_C \geq t^{(i)} \mid \mathbf{x}^{(i)})^{\delta^{(i)}} \times \Pr(T_E \geq t^{(i)}, T_C = t^{(i)} \mid \mathbf{x}^{(i)})^{1-\delta^{(i)}}. \quad (1)$$

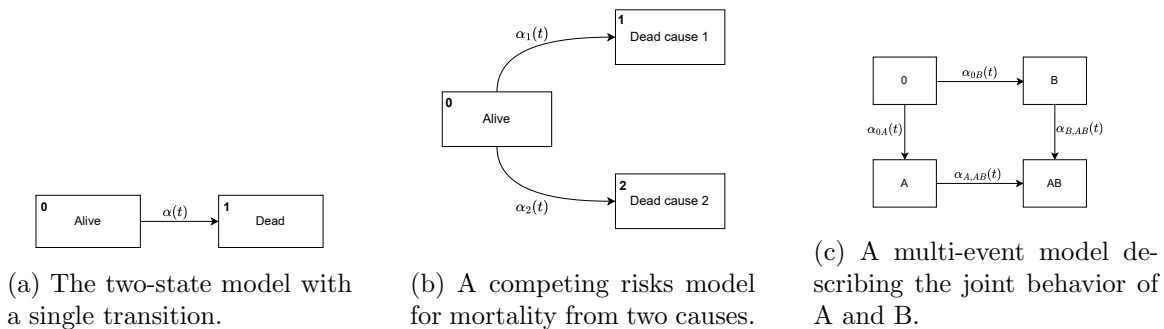


Figure 3: Event models for different scenarios.

3.2 Multi-state analysis

We now introduce a framework for examining multi-state models called *marked point processes* (Andersen and Keiding, 2002). A marked point process is a stochastic process $G(t)$, $t \in \mathcal{T}$ with a finite state space $\mathcal{P} = \{0, \dots, P-1\}$ and with right-continuous sample paths: $G(t+) = G(t)$. Here, $\mathcal{T} = [0, \tau]$ with $\tau \leq \infty$. The process has an initial distribution $\pi_p(0) = [\Pr(G(0) = p) \mid p \in \mathcal{P}]$. A multi-state process $G(\cdot)$ generates a history \mathcal{G}_t , which consists of observations of the process in the interval $[0, t]$ - *e.g.*, Mr. Smith is healthy at the start of the study ($\mathcal{G}_{t=0}$), but becomes ill 10 days later ($\mathcal{G}_{t=10}$), before the study terminates after 100 days ($\tau = 100$). Given this history, we can define the transition probabilities by:

$$\Pr_{pj}(s, t) = \Pr(G(t) = j \mid G(s) = p, \mathcal{G}_{s-}),$$

for $p, j \in \mathcal{P}, s, t \in \mathcal{T}, s \leq t$ and transition intensities by the derivatives, assuming such exist:

$$\alpha_{pj}(t) = \lim_{\Delta t \rightarrow 0} \frac{\Pr_{pj}(t, t + \Delta t)}{\Delta t}.$$

Some transition intensities may be 0 for all t between two states, *i.e.*, $\alpha_{pj}(t) = 0 \forall t$ and $\forall p, j \in \mathcal{P}$. A state $p \in \mathcal{P}$ is absorbing if, for all $t \in \mathcal{T}, j \in \mathcal{P}, j \neq p, h_{pj}(t) = 0$; otherwise p is transient. The state probabilities $\pi_p(t) = \Pr(G(t) = p)$ are given by:

$$\pi_p(t) = \sum_{j \in \mathcal{P}} \pi^j(0) \cdot \Pr_{jp}(0, t).$$

Note that the $\Pr_{pj}(\cdot, \cdot)$ and the $\alpha_{pj}(\cdot)$ depend on both the probability measure $\Pr(\cdot)$ and on the history, though our notation here omits these dependencies.

Competing risks. In competing risks, multiple events (*i.e.*, absorbing states) exist, but only one event (*i.e.*, state transition) can occur for each instance. A competing-risks model thus has one transient state, aka. state 0, and a number of absorbing states, K , *i.e.*, event k for $k \in \{1, \dots, K\}$. Thus, we have P total states and $K = P - 1$ event states (see Figure 3b). In this model, if an instance is censored before experiencing any events, it simply remained in the transient state and is thus event-free. The transition intensities $\alpha_{0k}(t)$ for $k \in \{1, \dots, K\}$ are given by the cause-specific hazard functions:

$$\alpha_k(t) = \lim_{\Delta t \rightarrow 0} \frac{\Pr(\text{Dead from cause } k \text{ at } t + \Delta t \mid T \geq t)}{\Delta t},$$

where T is the random variable corresponding to survival time (that is, time to event). The initial distribution is degenerate in 0, the only transient state of the model, *i.e.*, $\alpha_{kj}(t) = 0$ for all $k \neq 0$ and all j . The transition probabilities are given by the survival function:

$$\Pr_{00}(0, t) = S(t) = \Pr(T > t) = \exp\left(-\int_0^t \sum_{k=1}^K \alpha_k(u) du\right),$$

and the cumulative incidence function for transitioning from 0 to any $k \neq 0$:

$$\Pr_{0k}(0, t) = \int_0^t S(u-) \alpha_k(u) du, \quad k = 1, \dots, K.$$

Multi-event. In multi-event survival analysis, we can observe multiple events for each instance i , thus they are not mutually-exclusive. Figure 3c exhibits a multi-event model, which describes the behavior of two events A and B , and their joint event, AB . As an example, consider the probability that Mr. Smith will have the onset of pneumonia (A) and COVID-19 (B) at the same time. If the time until the onset of B does not depend on whether the patient has A – that is, $\alpha_{0B} = \alpha_{A,AB}$ – then A is called locally dependent on B . If the onset of A is different depending on whether the patient has B – that is, $\alpha_{0A} \neq \alpha_{B,AB}$ – then B is not locally dependent on A . Here, this temporal sequence of events thus provides asymmetric dependence between events (Andersen and Keiding, 2002).

4 The proposed method

4.1 Preliminaries

We now extend the previous single-event notation to a multi-event notation over P states. Let $\mathcal{D} = \{(\mathbf{x}^{(i)}, \mathbf{t}^{(i)}, \boldsymbol{\delta}^{(i)})\}_{i=1}^N$ be the dataset, where $\mathbf{x}^{(i)} \in \mathbb{R}^d$ is a d -dimensional vector of features, $\mathbf{t}^{(i)} \in \{1, 2, \dots, T_{\max}\}^K$ is a vector of observed times for the i -th person now across K multiple events, each at some time, and $\boldsymbol{\delta}^{(i)} \in \{0, 1\}^K$ is vector of event indicators for each event. Moreover, let $e_k^{(i)} \in \{1, 2, \dots, T_{\max}\}$ denote the event time and let $c_k^{(i)} \in \{1, 2, \dots, T_{\max}\}$ denote the censoring time for the i -th instance for event k over the event horizon, thus $t_k^{(i)} = e_k^{(i)}$ if $\delta_k^{(i)} = 1$, otherwise, $t_k^{(i)} = c_k^{(i)}$ if $\delta_k^{(i)} = 0$. We define a multi-event survival problem as predicting the probability of instance i experiencing event k at each time point $t \in \{1, 2, \dots, T_{\max}\}$. This produces a matrix of survival functions $\mathbf{S}^{(i)} = [\mathbf{s}_1^{(i)}, \mathbf{s}_2^{(i)}, \dots, \mathbf{s}_P^{(i)}]$ for instance i , where P is the number of states. Recall that the survival function is the probability that some event occurs at time T later than t – *i.e.*, $\mathbf{s}_p^{(i)} = [\Pr(e_p^{(i)} > 1), \Pr(e_p^{(i)} > 2), \dots, \Pr(e_p^{(i)} > T_{\max})]$ describes the probability that instance i does not transition to state p until t for $t \in \{1, 2, \dots, T_{\max}\}$.

As a practical example, consider a clinical trial over $t \in [0, 100]$ days. The trial tests a new drug that can give participants two possible side effects: “nausea” ($k = 1$) or “fatigue” ($k = 2$). In our multi-state framework with P states, let $P = 0$ denote the “event-free” state, let $P = 1$ denote the “nausea” state and let $P = 2$ denote the “fatigue” state in this example. We then encode the “event-free” state as $e_{p=0}^{(i)} = \max(t_k^{(i)} \mid \delta_k^{(i)} = 0)$ and $\delta_{p=0}^{(i)} = 1$, if i never experiences an event, otherwise, $e_{p=0}^{(i)} = \min(t_k^{(i)} \mid \delta_k^{(i)} = 1)$ and $\delta_{p=0}^{(i)} = 0$. We illustrate this notation in Figure 4, where $\delta_p^{(i)}$ is the event indicator and t_p is the observed time for state p . Basically, if the patient never has any events, he is event-free (*i.e.*, we observe the “event-free” event) at the time the last event was censored. If the patient has an event, then he is not event-free (*i.e.*, we did not observe the “event-free” event) at the time the first event was observed.

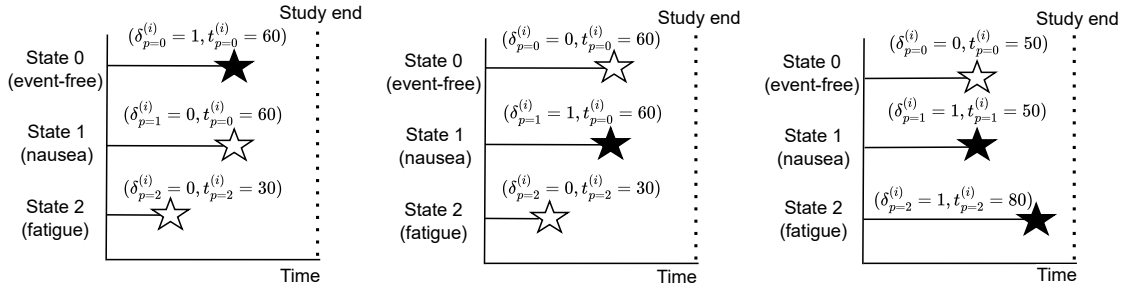


Figure 4: Example to illustrate our notation. Left: the patient i was event-free after 60 days. Center: the patient experienced nausea after 60 days. Right: the patient experienced nausea after 50 days and fatigue after 80 days.

Let us revisit our fictive patient, Mr. Smith. participates in the aforementioned clinical trial and enrolls in the study at baseline ($t = 0$) with his covariates $\mathbf{x}^{(i)}$. After taking the drug, Mr. Smith experienced nausea after 10 days and fatigue after 20 days, and was

never censored for any events (*i.e.*, we observed all events). Using the proposed multi-state notation, we would encode Mr. Smith’s event information as follows:

- **State 0:** $e_{p=0}^{(i)} = 10, \delta_{p=0}^{(i)} = 0$, indicating he stayed event-free until $t = 10$.
- **State 1:** $e_{p=1}^{(i)} = 10, \delta_{k=1}^{(i)} = 1$, indicating he had the “nausea” event at $t = 10$.
- **State 2:** $e_{p=2}^{(i)} = 20, \delta_{p=2}^{(i)} = 1$, indicating he had the “fatigue” event at $t = 20$.

4.2 Mixture model architecture

We propose to model the marginal survival distribution for each state – *i.e.*, the transition probability $P_{0p}(s, t)$ of entering that state over all states P – as a convex combination of $\Psi \in \mathbb{R}_+$ Weibull distributions. There are two reasons for this: (1) this approach relaxes the proportional hazard assumption about the underlying marginal survival distribution for each state, as a mixture architecture can model non-proportional hazard functions (see Appendix G for details); and (2) the Weibull distribution has a closed-form probability density function (PDF) and cumulative distribution function (CDF) as:

$$f(t; \beta, \eta) = \frac{\eta}{\beta} \left(\frac{t}{\beta}\right)^{\eta-1} \exp\left(-\left(\frac{t}{\beta}\right)^\eta\right),$$

$$F(t; \beta, \eta) = 1 - \exp\left(-\left(\frac{t}{\beta}\right)^\eta\right),$$

where $\beta > 0$ and $\eta > 0$ are the shape and scale parameters, respectively. The shape parameter models the skew of the distribution, and the scale parameter models the distribution spread, also referred to as the characteristic life. This closed form simplifies the gradient computation. Assuming our estimated survival distribution is a convex combination of Ψ Weibulls for each marginal distribution, we can define the log of β_ψ and η_ψ as:

$$\log\left(\beta_\psi(\mathbf{x}^{(i)})\right) = \tilde{\beta}_\psi + \text{act}\left(\Phi_\theta(\mathbf{x}^{(i)})^\top \zeta_\psi\right), \quad (2)$$

$$\log\left(\eta_\psi(\mathbf{x}^{(i)})\right) = \tilde{\eta}_\psi + \text{act}\left(\Phi_\theta(\mathbf{x}^{(i)})^\top \xi_\psi\right). \quad (3)$$

Here, $\mathbf{x}^{(i)} \in \mathbb{R}$ is the input vector of feature values describing the i -th instance, and $\Phi_\theta(\cdot)$ is a feature representation layer, which is shared among events. This layer accounts for inter-event dependencies captured in the features. The other terms are specific to each output event. The parameters $\tilde{\beta}_\psi \in \mathbb{R}$ and $\tilde{\eta}_\psi \in \mathbb{R}$ are learnable log-scale biases that initialize the log-transformed scale and shape parameters, respectively, for the ψ -th component. $\text{act}(\cdot)$ is a non-linear activation function, in our case SELU (Klambauer et al., 2017). Finally, ζ_ψ and ξ_ψ are learnable weight vectors for the scale and shape parameters, respectively, of the ψ Weibull distribution. As a result, we can define the PDF and CDF for each marginal as:

$$f\left(t; \beta, \eta, \mathbf{x}^{(i)}\right) = \sum_{\psi=1}^{\Psi} g_\psi(\mathbf{x}^{(i)}) f_\psi\left(t; \beta_\psi(\mathbf{x}^{(i)}), \eta_\psi(\mathbf{x}^{(i)})\right), \quad (4)$$

$$F\left(t; \beta, \eta, \mathbf{x}^{(i)}\right) = \sum_{\psi=1}^{\Psi} g_\psi(\mathbf{x}^{(i)}) F_\psi\left(t; \beta_\psi(\mathbf{x}^{(i)}), \eta_\psi(\mathbf{x}^{(i)})\right), \quad (5)$$

where $g_\psi = \text{Softmax}(\Phi_\theta(\mathbf{x}^{(i)})^\top g_\theta)$ is a weighting function that determines the contribution of each ψ distribution to the marginal distribution. For computational efficiency, we calculate the sum of the logarithms of the weighting function and the density functions, respectively. Figure 5 shows the proposed architecture; a neural network with a transient state and multiple event states, where each state models the (marginal) probability of observing (transitioning to) state p at time t , out of $P \in \mathbb{Z}^{\geq 0}$ state transitions, given parameters $(\hat{\beta}_{\psi,p}, \hat{\eta}_{\psi,p})$, and some (latent) feature representation $\tilde{\mathbf{x}}^{(i)}$. For each instance, the model predicts $\mathbf{S}^{(i)} = [s_0^{(i)}, s_1^{(i)}, \dots, s_{P-1}^{(i)}]$, that is, a matrix of probability distributions, where the p -th represents the probability of entering the p state at time T later than t (for each $t > 0$).

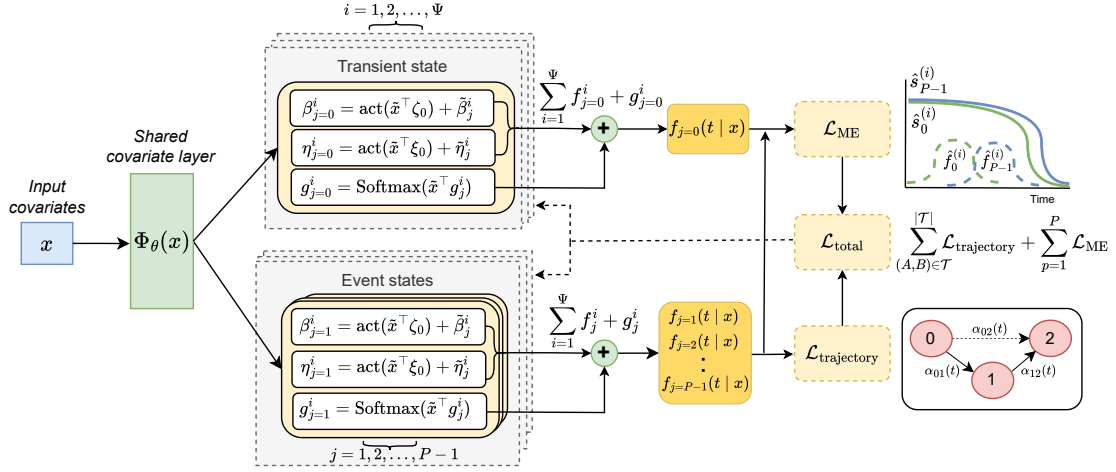
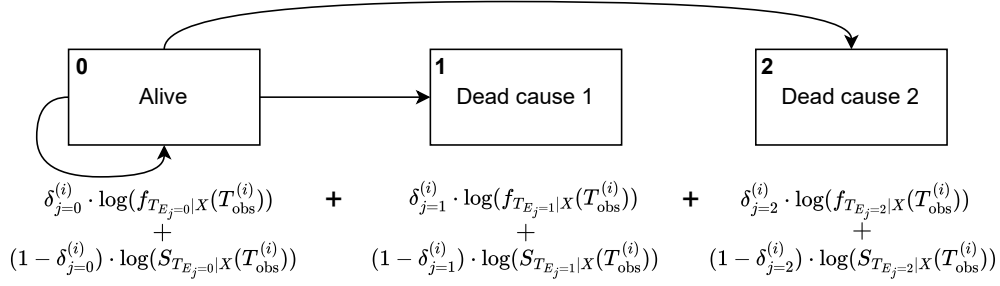


Figure 5: An illustration of the proposed network architecture for MENSA.

4.3 Competing-risks likelihood

Given survival data $\mathcal{D} = \{(X^{(i)}, T^{(i)}, \delta^{(i)})\}_{i=1}^N$, recall that $f_{T_E|X}(\cdot)$ represents the conditional density function, where T_E is the event distribution. In order to estimate Eqs. (2) and (3) using MLE, we adopt the likelihood in Eq. (1) to the competing-risks scenario under the conditional independence assumption, now using the survival function $S_{T|X}(\cdot)$, which represents the likelihood that the event (or censoring) will take place after the argument time t . This approach mimics the one in DSM (Nagpal et al., 2021), however, we also consider the event-free state (*i.e.*, the transient state) as an event in the likelihood function by calculating the likelihood across P states instead of K events. Figure 6 shows an example of the likelihood composition based on the previous competing-risks model in Figure 3b.

This explicitly models the probability of staying event-free (*i.e.*, not experiencing any of K events) for instance i over the event horizon $[0, \dots, t_{\max}]$, and thus allows us to “predict” the event-free (transient) distribution, *i.e.*, will the instance i remain event-free over the follow-up period or experience one of K events. Our approach also differs from Nagpal et al. (2021) as we optimize the log-likelihood directly instead of deriving a lower bound on it. Given the survival dataset \mathcal{D} with N instances and K competing risks, where $\delta_j^{(i)}$ indicates the event indicator for j th state for the i th instance, we can write the composite likelihood

Figure 6: Composition of the log-likelihood under competing risks over P states.

as follows (see also Figure 6):

$$\mathcal{L}_{\text{CR}}(\mathcal{D}) = \prod_{i=1}^N \prod_{j=1}^P f_{T_{E_j}|X}(T_{\text{obs}}^{(i)} | X^{(i)})^{\delta_j^{(i)}} \cdot S_{T_{E_j}|X}(T_{\text{obs}}^{(i)} | X^{(i)})^{1-\delta_j^{(i)}}.$$

In practice, we optimize the joint log-likelihood function, which has the following form:

$$\mathcal{L}_{\text{CR}}(\mathcal{D}) = \sum_{i=1}^N \sum_{j=1}^P \delta_j^{(i)} \log \left(f_{T_{E_j}|X} \left(T_{\text{obs}}^{(i)} | X^{(i)} \right) \right) + (1 - \delta_j^{(i)}) \log \left(S_{T_{E_j}|X} \left(T_{\text{obs}}^{(i)} | X^{(i)} \right) \right). \quad (6)$$

4.4 Multi-event likelihood with trajectories

We now extend our model to the multi-event scenario, where events (*i.e.*, state transitions) can happen in any order and at any time, and are not necessarily mutually-exclusive. To this end, we can simply extend Eq. 6 to a multi-state scenario as a composite likelihood function over the P states, with different observed times for the different state transitions, omitting the log-operation for brevity:

$$\mathcal{L}_{\text{ME}}(\mathcal{D}) = \sum_{i=1}^N \sum_{j=1}^P \left[\delta_j^{(i)} f_{T_{E_j}|X} \left(T_{\text{obs}(j)}^{(i)} | X^{(i)} \right) + (1 - \delta_j^{(i)}) S_{T_{E_j}|X} \left(T_{\text{obs}(j)}^{(i)} | X^{(i)} \right) \right], \quad (7)$$

which differs from Eq. 6 only by using $T_{\text{obs}(j)}^{(i)}$, which now indicates the observed time for j th state transition – *i.e.*, instance i was last observed in state j at time $T_{\text{obs}(j)}^{(i)}$. This likelihood mimics the likelihood in Tjandra et al. (2021), who calculated the event-specific likelihood over K events, not considering the event-free state nor the temporal ordering between events. However, many real-world events do not happen in isolation, but have some relationship to each other in time.

An example is the illness-death model (Fix and Neyman, 1951), where patients start out healthy (state 0) and then may become ill (event A) and go on to die (event B). In general, there are four possible scenarios for two events at any specific time: (1) Neither event A nor B has happened (*i.e.*, both are censored), (2) only event A happened (but B is censored),

(3) only event B has happened (but A is censored), and (4) both events happened, and event A occurred before event B, *i.e.*, the patient became ill and then died. In the last case, we have a known ordering of events, assuming that patients who experience both A and B must first become ill and then die. (Note that we do **not** consider the possibility of people dying before the onset of a disease in this example).

To incorporate this ordering into our optimization algorithm, we want to construct a likelihood that maximizes $S_B(t_A)$, *i.e.*, the survival probability associated with event B at the time of event A, t_A . This ensures that when event A occurs, the model assigns a high probability that event B has not yet occurred, effectively enforcing that event B is likely to occur after event A. This encourages the model to assign a high survival probability for event B at the time when event A occurs, effectively enforcing a known temporal ordering between events.

#	δ_A	δ_B	Transition prob.	Log-likelihood
1	0	0	$1 - (P_{0A}(t_A) + P_{0B}(t_B))$	$S_A(t_A) + S_B(t_B)$
2	1	0	$P_{0A}(t_A)$	$f_A(t_A) + S_B(t_B)$
3	0	1	$P_{0B}(t_B)$	$S_A(t_A) + f_B(t_B)$
4	1	1	$P_{0A}(t_A) * P_{0B}(t_B)$	$f_A(t_A) + f_B(t_B) + \mathbf{S}_B(\mathbf{t}_A)$

Table 1: List of possible scenarios considering two events, A and B. If we can establish, based on prior knowledge, that if both events occur, then event A must have occurred before event B, we can add the probability of surviving event B at the time of event A to the overall likelihood, as shown in the bottom row.

Formally, we define a trajectory set $\mathcal{T} = \{(A, B) \mid A, B \in \mathcal{K}, A \text{ occurs before } B\}$, which consists of ordered pairs of events (A, B) drawn from the set of all events, \mathcal{K} , where it is known that event A must occur before event B, whenever both events are observed. For example, if a person becomes ill and later dies, they must have first experienced illness before death. To incorporate this ordering of events into our likelihood function, we introduce a trajectory likelihood denoted $\mathcal{L}_{\text{trajectory}}$ (see Eq. 8); for patient i , we consider all event pairs in a set of trajectories \mathcal{T} where both events are uncensored – *i.e.*, both events are observed. The trajectory likelihood is computed by summing the survival probability of event B at the time of event A, thus $S_B(T_A \mid X^{(i)})$, weighted by the event indicators $\delta_A^{(i)}$ and $\delta_B^{(i)}$, which equal 1 if events A and B have occurred for patient i , respectively, and 0 otherwise. This encourages the model to assign a high survival probability for event B at the time when event A occurs, effectively enforcing a known temporal ordering between events. We can write this trajectory likelihood as:

$$\mathcal{L}_{\text{trajectory}}(\mathcal{D}) = \sum_{i=1}^N \sum_{(A,B) \in \mathcal{T}} S_B(T_A \mid X^{(i)}) \cdot \delta_A^{(i)} \cdot \delta_B^{(i)}, \quad (8)$$

where \mathcal{T} is a set of possible trajectories. Finally, we add the weighted likelihoods together:

$$\mathcal{L}_{\text{total}}(\mathcal{D}) = \frac{1}{N} \mathcal{L}_{\text{ME}}(\mathcal{D}) + \frac{1}{N} \mathcal{L}_{\text{trajectory}}(\mathcal{D}).$$

Algorithm 1 shows the proposed optimization algorithm.

Algorithm 1 The proposed optimization algorithm for MENSA.

- 1: **Input:** A survival dataset \mathcal{D} of the form $\{(X^{(i)}, T_{\text{obs}}^{(i)}, \delta^{(i)})\}_{i=1}^N$; \mathcal{M} : the model with default initialized parameters $\{\Phi_\theta, \tilde{\beta}, \tilde{\eta}, \zeta, \xi, g_\theta\}$; \mathcal{T} : list of trajectories; λ : learning rate; L : number of training epochs (learning iterations).
 - 2: **Result:** $\mathcal{M} = \{\hat{\Phi}_\theta, \hat{\beta}, \hat{\eta}, \hat{\zeta}, \hat{\xi}, \hat{g}_\theta\}$: The model with learned parameters.
 - 3: **Initialization:**
 $\mathcal{M} \leftarrow \text{Instantiate}(\mathcal{M}; \hat{\Phi}_\theta^{(0)}, \hat{\beta}^{(0)}, \hat{\eta}^{(0)}, \hat{\zeta}^{(0)}, \hat{\xi}^{(0)}, \hat{g}_\theta^{(0)})$
 - 4: **for** $i = 1, \dots, L$ **do**
 - 5: $f(T_{\text{obs}}), S(T_{\text{obs}}) \leftarrow \mathcal{M}(\mathcal{D})$ // f and S are $N \times P$
 - 6: $\mathcal{L}_{\text{ME}} \leftarrow \ell(\delta_{n=1}^N, f(T_{\text{obs}}), S(T_{\text{obs}}))$ // NLL across P states
 - 7: $\mathcal{L}_{\text{trajectory}} \leftarrow 0$
 - 8: **for** each pair $(a, b) \in \mathcal{T}$ **do**
 - 9: $\mathcal{L}_{\text{trajectory}} += \ell(a, b, \delta_{n=1}^N, S(T_{\text{obs}}))$ // Accumulate trajectory likelihood
 - 10: **end for**
 - 11: $\mathcal{L}_{\text{total}} \leftarrow \frac{1}{N} \mathcal{L}_{\text{ME}} + \frac{1}{N} \mathcal{L}_{\text{trajectory}}$ // Sum the weighted likelihoods
 - 12: $\{\hat{\Phi}_\theta, \hat{\beta}, \hat{\eta}, \hat{\zeta}, \hat{\xi}, \hat{g}_\theta\}^{(i)} \leftarrow \text{SGD}(\{\hat{\Phi}_\theta, \hat{\beta}, \hat{\eta}, \hat{\zeta}, \hat{\xi}, \hat{g}_\theta\}^{(i-1)}, \mathcal{L}_{\text{total}}, \lambda)$ // Optimization step
 - 13: **end for**
 - 14: **return** \mathcal{M}
-

5 Experimental setup

5.1 Implementation

The backbone network architecture for our mixture model is a multilayer perceptron (MLP) — a fully connected feedforward network with several hidden layers and a nonlinear activation function for all nodes. The use of an MLP is consistent with the literature, showing strong predictive performance (Katzman et al., 2018; Nagpal et al., 2021; Lillelund et al., 2024b). For all experiments, we use a single layer with $\{32, 64, 128\}$ nodes and the ReLU6 activation function. We train MENSA with the Adam optimizer (Kingma and Ba, 2017), and use learning rates of $\lambda \in \{1e-3, 5e-4, 1e-4\}$ for the MLP, and $\Psi \in \{1, 3, 5\}$ number of Weibull distributions for each event. We add regularization using weight decay of $\{1e-3, 5e-3, 1e-2\}$ and dropout rates of $\{0, 0.1, 0.25, 0.5\}$ with batch normalization. Training is done using minibatches, *i.e.*, stochastic subsets of the training dataset with sizes of $\{32, 64, 128\}$. We use hyperparameter optimization on the validation set, for each of these hyperparameters We provide additional details on implementation in Appendix F.

For evaluation fairness, we configure all baseline models with sensible default parameters; for neural network models, we use a single hidden layer with 32 nodes. For models that support it, we use early stopping during training to terminate the process if the validation likelihood loss does not improve for 10 consecutive epochs. We provide further details on the hyperparameters for MENSA and the baseline models in Appendix E.

Concerning the empirical experiments, we evaluate all models over 10 experiments by applying different survival baselines to six survival datasets with different random seed (0-9) to ensure variability. In each experiment, we follow Sechidis et al. (2011) and first split the dataset into training (70%), validation (10%), and test (20%) sets in a stratified

manner wrt the event indicators and event times across the K events given a random seed. The stratification ensures a balanced representation of the time-to-event information and outcome across the data splits. After splitting, we impute missing values using the sample mean for real-valued features or the mode for categorical features based on the training set only. We then apply a z -score data normalization to speed up the training process and improve stability. Lastly, we encode categorical features using a one-hot encoding strategy.

5.2 Datasets

This section briefly describes the survival datasets in this work. Table 2 shows an overview of the datasets. We provide further details on the data and preprocessing in Appendix D.

Dataset	#Instances (N)	#Features (d)	#Events (K)	Max t	Event distribution (%)
Synthetic*	10,000	100	1	285	C: 30.4, E: 69.6
SEER*†	19,246	17	1/2	121	D: 45.5 BC: 12.4, HF: 45.5
MIMIC-IV*‡	24,516	100	1/3	4,686	D: 37.2 A: 20.7, S: 19.2, D: 37.2
Rotterdam†‡	2,982	10	2/3	7,043	R: 6.5, D: 50.9 R: 50.9, D: 42.7
PRO-ACT‡	3,220	8	4	498	SP: 37.8, SW: 31.9, HA: 50.3, WA: 60.6
EBMT‡	2,279	6	5	6229	R: 34.4, AE: 39.8, RAE: 29, REL: 16.2, D: 23.4

Table 2: Overview of the raw datasets. Symbols indicate single-event (*), competing-risks (†) or multi-event (‡) task. Number of events (K) is denoted for the respective task. In SEER, “D”, “BC” and “HF” denote the death event, death by breast cancer and death by heart failure. In MIMIC-IV, “A”, “S”, and “D” denote the ARF, shock and death events. In Rotterdam, “R” denotes relapse and “D” denotes death. In Rotterdam, “R” means relapse and “D” means death. In PRO-ACT, “SP”, “SW”, “HA” and “WA” denote the speech, swallowing, handwriting and walking events. In EBMT, “R”, “AE”, “RAE”, “REL” and “D” denote the recovery, adverse events, recovery and adverse events, relapse, and death events.

Synthetic: Following Foomani et al. (2023), we create synthetic, single-event datasets from a data generation process (DGP) with a linear or nonlinear activation function. To evaluate our model under dependent censoring, *i.e.*, where the event and censoring times are not independent, we sample T_E and T_C R.V.s from a so-called *copula*. A copula $C_\theta(u, v)$ links R.V.s by specifying their dependence structure (Emura and Chen, 2018, Ch. 1). Applied here, it captures the dependency (Kendall’s τ) between T_E and T_C by sampling the marginals from a (survival) copula. If $\tau = 0$, the marginals are generated as independent uniform R.V.s, otherwise, they are generated using an Archimedean copula. We provide more details about this data generation process in Appendix D.

SEER: The U.S. Surveillance, Epidemiology, and End Results (SEER) dataset (Ries et al., 2003) is a comprehensive collection of cancer patient data from approximately 49% of the U.S. population. It provides information about survival times for cancer patients post diagnosis. We select a cohort of 19,246 newly-diagnosed patients (first year of disease) with 17 features, which include demographics and tumor characteristics. For the single-event case, we consider the outcome of death due to breast cancer, and for the competing-risks case, we consider the outcomes of death due to breast cancer and death due to heart failure – and consider other outcomes as censored.

MIMIC-IV: The Medical The Information Mart for Intensive Care (MIMIC-IV) dataset by Johnson et al. (2023) comprises electronic health records from patients admitted to intensive care units at the Beth Israel Deaconess Medical Center in the U.S., covering the years from 2008 to 2019. Using the method described in Gupta et al. (2022), we extract 1,672 static features from the MIMIC-IV dataset, for 26,236 patients whose age is between 60 and 65 years. To refine our feature set, we apply the uniox feature selection method (Qi et al., 2022; Simon et al., 2003), reducing the number of features to the 100 that appear to be the most relevant (see Appendix D for details). For the single-event case, we consider death since hospital admission and for the multi-event case, we consider the outcomes of acute respiratory failure (ARF), shock and death.

Rotterdam: The Rotterdam dataset (Royston and Altman, 2013) includes 2,982 primary breast cancer patients from the Rotterdam tumor bank, with 1,546 having node-positive disease. The follow-up time ranged from 1 to 231 months (median 107 months). The dataset has 10 features, which include demographics, tumor characteristics, and treatment information. In the competing-risks case, we consider the outcome of recurrence-free survival time (RFS), which is defined as the time from primary surgery to the earlier of disease recurrence or death from any cause. In the multi-event case, we consider the time to death or disease recurrence, where death censors disease recurrence, but disease recurrence does not censor death. Figure 7 shows the event trajectories in the Rotterdam dataset.

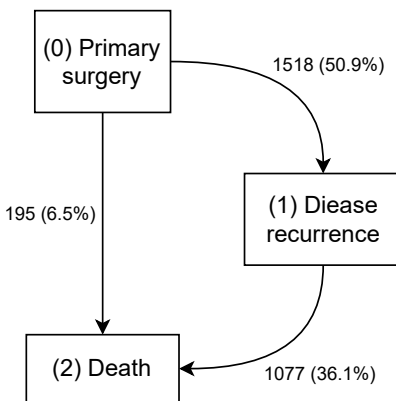


Figure 7: Event trajectories in the Rotterdam dataset ($N=2,982$).

PRO-ACT: The Pooled Resources Open-Access Clinical Trials (PRO-ACT)¹ database by Atassi et al. (2014) is the largest ALS dataset in the world, which includes patient demographics, lab and medical records and family history of over 11,600 ALS patients, where ALS disease state is evaluated by the ALS functional rating scale revised (ALSFRS-R). The assessment contains 12 questions and a maximum score of 48, each representing physical functionality, *e.g.*, the ability to walk. Each ALSFRS-R score is between 0 and 4, where 0 represents complete inability with regard to the function, and 4 represents normal function. We use the ALSFRS-R scores to formulate four events: “Speech”, “Swallowing”, “Handwriting” and “Walking”. We consider an event to have occurred if a patient scores 2 or lower on the ALSFRS-R scale during any subsequent follow-up visitation following their baseline visitation. The events can occur in any order and are not mutually exclusive. ALSFRS-R scores are generally monotonic decreasing, but due to the subjectivity of the assessment, scores can occasionally increase post-baseline. We use a maximum follow-up time of 500 days and exclude patients with no recorded history.

EBMT: The European Society for Blood and Marrow Transplantation (EBMT) dataset (Marta Fiocco, 2008) contains records of 2,279 patients who underwent blood and marrow transplantation between 1985 and 1998 for acute lymphoid leukemia. The dataset has several features, including gender mismatch between donor and recipient, age at transplant, whether any GvHD prophylaxis was administered, and year of transplantation. We consider five events: platelet recovery from acute-graft-versus-host disease (AGvHD), adverse effects after transplantation, recovery and adverse effects, disease relapse and death in remission. If AGvHD occurs, it will occur shortly after the transplant, usually within the first 100 days. Figure 8 shows the event trajectories in the EBMT dataset.

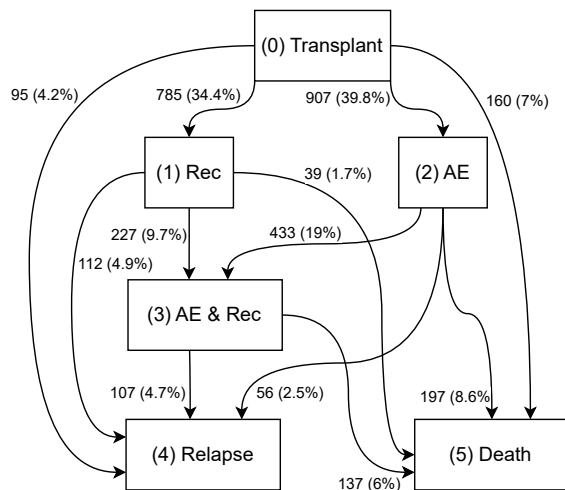


Figure 8: Event trajectories in the EBMT dataset ($N=2,279$).

1. Data used in the preparation of this article were obtained from the Pooled Resource Open-Access ALS Clinical Trials (PRO-ACT) Database. The data available in the PRO-ACT Database have been volunteered by PRO-ACT Consortium members.

5.3 Baseline models

CoxPH: The Cox Proportional Hazards model (CoxPH) is a shallow semiparametric model for survival analysis (Cox, 1972). The conditional individual hazard function assumed by the CoxPH model is $h(t|\mathbf{x}^{(i)}) = h_0(t) \exp(f(\boldsymbol{\theta}, \mathbf{x}^{(i)}))$, where $h_0(t)$ is the baseline hazard at t , $f(\boldsymbol{\theta}, \mathbf{x}^{(i)})$ is a risk score, and f is a linear function. Its standard MLE of $\hat{\boldsymbol{\theta}}$ optimizes the so-called Cox partial log-likelihood (Cox, 1972).

GBSA: GBSA (Ridgeway, 1999) is a shallow likelihood-based boosting model that optimizes an ℓ_2 -norm penalized Cox partial log-likelihood (Cox, 1972). It updates candidate variables flexibly at each boosting step using an offset-based gradient boosting method, unlike traditional gradient boosting, which updates either a single component or all features for fitting the gradient.

RSF: Random Survival Forests (RSF) (Ishwaran et al., 2008) extends decision trees for survival analysis and recursively splits training data based on some survival-specific criterion, *e.g.*, log-rank splitting, with the goal of maximizing separation between survival times across nodes.

DeepSurv: DeepSurv (Katzman et al., 2018) is a deep continuous-time survival model of the form $h(t|\mathbf{x}^{(i)}) = h_0(t) \exp(f(\boldsymbol{\theta}, \mathbf{x}^{(i)}))$, where $f(\boldsymbol{\theta}, \mathbf{x}^{(i)})$ denotes a risk score as a nonlinear function of the features, *i.e.*, $f(\boldsymbol{\theta}, \mathbf{x}^{(i)}) = \sigma(\mathbf{x}^{(i)}\boldsymbol{\theta})$. The MLE for $\hat{\boldsymbol{\theta}}$ is derived by numerically maximizing the partial Cox log-likelihood.

DeepHit: DeepHit (Lee et al., 2018) is a deep discrete-time model designed to handle competing risks, where the occurrence of one event prevents the occurrence of another, as it assumes $\sum_{t=1}^T \sum_{k=1}^K p_k[t] = 1$. It features a shared subnetwork among all events and cause-specific subnetworks for each competing event. The model outputs a probability distribution for each discrete time bin and each competing event via a softmax layer. This architecture allows DeepHit to estimate the joint distribution of survival times and events directly without making assumptions about the underlying stochastic process. It accounts for dependencies among events in $\boldsymbol{\theta}$ but not for individuals who are event-free at time T .

Hierarchical: The hierarchical model (Tjandra et al., 2021) is a deep discrete-time model designed to handle multi-event. The model learns the individual survival distribution by iteratively predicting the probability of an event at increasingly finer time scales. During training, the model uses a composite likelihood function using ranking penalties that provide supervision across the entire event horizon.

MTLR: The Multi-Task Logistic Regression (MTLR) model (Yu et al., 2011) is a discrete-time survival model that predicts the survival distribution using a sequence of dependent logistic regressors. The MTLR model has been extended to the competing-risks case as the Deep-CR MTLR model by Kim et al. (2021).

DSM: Deep Survival Machines (DSM) (Nagpal et al., 2021) is a deep continuous-time model that estimates the survival distribution as a mixture of some fixed k parametric distributions. The parameters of these mixture distributions and the mixing weights are estimated using an MLP.

We configure all baseline models with sensible defaults, which are in Appendix E.

5.4 Evaluation metrics

For the single-event datasets, we evaluate discrimination using the traditional **Harrell’s concordance index (CI)** (Harrell Jr. et al., 1982). In the competing-risks and multi-event datasets, we report the **Global CI** as the average of the CIs across events, and the **Local CI**, as the average of the CIs for each individual. Thus, these two discrimination metrics evaluate global consistency, *i.e.*, how well does the model discriminate individuals *within* an event, and local consistency, *i.e.*, how well does the model discriminate events *within* an individual. Figure 9 shows an example of this with respect to the survival curve. Visually, global consistency is satisfied between instances if the instance-specific curves align with the observed events. Local consistency is satisfied within an instance if the event-specific curves align with the observed events. We evaluate the accuracy of the predicted time-to-event estimates using mean absolute error (MAE) with a margin loss for censored individuals (**mMAE**) (Haider et al., 2020) and the integrated Brier Score (**IBS**) (Graf et al., 1999). To evaluate calibration, we report the Distribution-Calibration (**D-Cal**) score (Haider et al., 2020), which measures how well the survival function is calibrated for each event. Lastly, we evaluate the bias induced by dependent censoring using the Survival- ℓ_1 error (Foomani et al., 2023), which is the ℓ_1 distance between the ground truth survival curve and the estimated survival curve. See Appendix B for more details about the evaluation metrics.

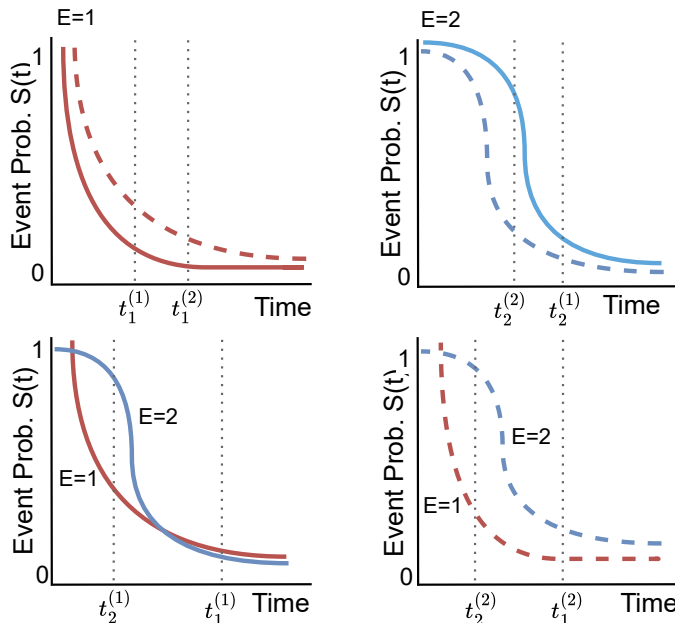


Figure 9: Global and local consistency. Red/blue lines represent survival functions $S_1(t)$ and $S_2(t)$ for event 1 and 2, respectively. Solid/dashed lines represent individuals $i = 1, 2$, respectively. Top-left: globally consistent at $t_1^{(1)}$ and $t_1^{(2)}$ since $S_1^{(1)}(t) < S_2^{(2)}(t)$ both times. Top-right: globally consistent at $t_2^{(2)}$ and $t_2^{(1)}$ since $S_2^{(2)}(t) < S_2^{(1)}(t)$ both times. Bottom-left: locally inconsistent at $t_2^{(1)}$ since $S_2^{(1)}(t) > S_1^{(1)}(t)$ and at $t_1^{(1)}$ since $S_1^{(1)}(t) > S_2^{(1)}(t)$. Bottom-right: locally inconsistent at $t_2^{(2)}$, since $S_2^{(2)}(t) > S_1^{(2)}(t)$.

6 Experiments and results

6.1 Single-event prediction

We first consider the single-event case ($K = 1$), and evaluate our method under dependent censoring. Dependent censoring occurs when the likelihood of being censored is related to the event time, which violates the key assumption of independent censoring behind covariate-based survival models (Emura and Chen, 2018, Ch. 3). Models that assume independence may therefore underestimate or overestimate the survival function due to the mismatch between the observed and true survival distributions. To investigate our method under dependent censoring, we train MENSA and baseline models on synthetic datasets with either linear or nonlinear Weibull hazards and with various degrees of dependence from either a Frank or Clayton copula. Figure 10 shows the performance results in terms of the bias (Survival- ℓ_1) for MENSA and baseline models under dependent censoring. In the linear case, we see that MENSA has one of the lowest Survival- ℓ_1 errors, and that its error is stable as a function of the dependence. In the nonlinear case, MENSA has above average error using a Frank copula but the second lowest error using a Clayton copula. This suggests that MENSA is robust to dependent censoring in the linear case under the assumption of dependence from a Frank or Clayton copula, and has lower estimation bias in the nonlinear case than all rival methods, except DeepHit, under a Clayton copula.

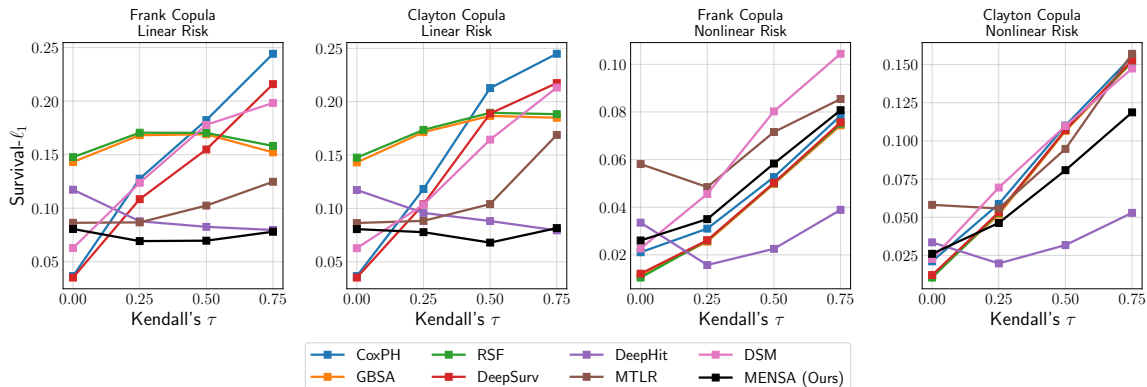


Figure 10: Plot of Survival- ℓ_1 as a function of Kendall's τ , *i.e.*, the dependence between T_E and T_C (see Appendix C). The lines represent the Survival- ℓ_1 means over 10 experiments. Lower is better.

We now evaluate MENSA in the SEER and MIMIC-IV datasets with a single event of interest ($K = 1$). Table 3 shows the prediction results. We see that MENSA consistently ranks among the best performing models in these two datasets. In the SEER dataset, MENSA exhibits good discriminative performance as it achieves the second-best (second-highest) Harrell's concordance index, slightly below the GBSA model. At the same time, MENSA has the best (lowest) integrated Brier Score and the second-best (second-lowest) margin MAE, highlighting its ability to make accurate survival predictions. MENSA also gives D-calibrated survival curves in 9 of 10 experiments, which is the highest number. In the MIMIC-IV dataset, MENSA also achieves good performances, as it has the best (highest) Harrell's concordance index, the best (lowest) Brier Score and second-best (second-

lowest) margin MAE, only surpassed by CoxPH in this regard. MENSA is D-calibrated in all ten MIMIC-IV experiments. These results suggest that MENSA is effective for both discrimination and prediction tasks in large, single-event datasets, and that it offers a good balance between discrimination (concordance index), prediction accuracy (Brier Score and MAE) and calibration performance (D-Calibration) in this case.

Dataset	Model	Harrell’s CI \uparrow	IBS \downarrow	mMAE \downarrow	D-Cal \uparrow
SEER ($N = 19,246$, $K = 1, d = 17$)	CoxPH	69.80 \pm 0.62	16.81 \pm 0.30	29.97 \pm 0.39	4/10
	GBSA	76.03\pm0.67	15.20 \pm 0.28	26.44\pm0.41	0/10
	RSF	74.53 \pm 0.58	16.96 \pm 0.25	27.84 \pm 0.27	0/10
	DeepSurv	74.75 \pm 1.11	15.29 \pm 0.40	28.37 \pm 0.61	1/10
	DeepHit	74.80 \pm 0.68	17.24 \pm 0.42	28.96 \pm 0.76	0/10
	MTLR	69.72 \pm 0.85	16.78 \pm 0.47	32.13 \pm 1.36	5/10
	DSM	75.38 \pm 1.14	15.15 \pm 0.51	44.75 \pm 5.42	3/10
	MENSA (Ours)	75.82 \pm 0.61	14.91\pm0.31	26.93 \pm 0.69	9/10
MIMIC-IV ($N = 24,516$, $K = 1, d = 100$)	CoxPH	74.24 \pm 0.48	12.85 \pm 0.38	5.94\pm0.03	10/10
	GBSA	72.79 \pm 0.49	14.43 \pm 0.40	6.26 \pm 0.06	10/10
	RSF	71.51 \pm 0.57	15.24 \pm 0.42	6.68 \pm 0.04	10/10
	DeepSurv	74.87 \pm 0.48	12.48 \pm 0.38	6.57 \pm 0.11	10/10
	DeepHit	74.13 \pm 0.47	14.06 \pm 0.41	6.62 \pm 0.18	0/10
	MTLR	71.78 \pm 0.47	13.33 \pm 0.32	8.58 \pm 2.74	0/10
	DSM	74.96 \pm 0.51	12.58 \pm 0.38	6.44 \pm 0.15	9/10
	MENSA (Ours)	75.36\pm0.50	12.39\pm0.38	6.08 \pm 0.08	10/10

Table 3: Single-event prediction results. We report the mean (\pm SD.) averaged over 10 experiments. D-calibration counts the number of times the respective model was D-calibrated. To improve readability, we have multiplied the CI and IBS by 100 and divided the mMAE results in MIMIC-IV by 100.

6.2 Competing-risks prediction

We now consider the competing-risks case ($K > 1$), where the K events are mutually exclusive — that is, each instance can have (at most) one event. We evaluate MENSA in the SEER and Rotterdam test sets. Table 4 shows the prediction results. In the SEER dataset, MENSA achieves the best (highest) global concordance index and the third-best (third-highest) local concordance index. MENSA also shines in giving accurate time-to-event predictions in this dataset, as MENSA has the best (lowest) integrated Brier Score and best (lowest) margin MAE, and achieves perfect D-calibration in all 20 experiments. Again, this highlights MENSA’s applicability in multiple event scenarios, where our interest extends beyond ranking and predicting individuals at risk for a single event to include multiple events. In the Rotterdam dataset, MENSA is again very competitive, as it achieves the best (highest) global concordance index and the second-best (second-highest) local concordance index, slightly behind DeepHit in the latter case. Although MENSA’s integrated Brier Score of 15.03 is slightly behind several competitors, it gives D-calibrated survival curves in 18/20 experiments and a margin MAE of 49.56, which is better than all rival models, except DeepHit. As evidenced by the calibration results, MENSA more often give calibrated survival curves than literature baselines in these two datasets.

Dataset	Model	Global CI \uparrow	Local CI \uparrow	IBS \downarrow	mMAE \downarrow	D-Cal \uparrow
(SEER $N = 19,246$, $K = 2, d = 17$)	DeepSurv	71.93 \pm 1.21	79.40 \pm 0.66	12.60 \pm 2.75	26.03 \pm 2.55	11/20
	DeepHit	71.35 \pm 0.50	78.51 \pm 0.70	13.87 \pm 3.34	75.52 \pm 47.30	0/20
	Hierarch.	71.05 \pm 0.98	70.49 \pm 0.97	15.85 \pm 0.19	36.77 \pm 9.80	0/20
	MTLR-CR	65.68 \pm 0.92	72.71 \pm 3.49	15.86 \pm 2.07	39.04 \pm 6.18	0/20
	DSM	72.54 \pm 1.26	79.45\pm0.47	12.61 \pm 2.54	69.92 \pm 24.12	14/20
	MENSA (Ours)	72.69\pm0.64	78.85 \pm 0.62	12.37\pm2.56	26.01\pm1.21	20/20
(Rotterdam $N = 2,982$, $K = 2, d = 10$)	DeepSurv	68.88 \pm 1.59	88.32 \pm 1.86	14.09\pm7.49	118.17 \pm 92.70	20/20
	DeepHit	64.36 \pm 1.73	88.98\pm1.53	14.85 \pm 7.35	31.23\pm2.80	5/20
	Hierarch.	63.66 \pm 1.61	74.30 \pm 2.43	76.17 \pm 20.19	83.40 \pm 41.87	0/20
	MTLR-CR	68.92 \pm 1.41	86.52 \pm 2.14	15.91 \pm 6.70	52.50 \pm 24.49	5/20
	DSM	69.24 \pm 1.76	86.43 \pm 3.12	14.35 \pm 5.98	133.30 \pm 13.87	15/20
	MENSA (Ours)	69.53\pm1.74	88.68 \pm 1.72	15.03 \pm 5.89	49.56 \pm 22.96	18/20

Table 4: Competing risks prediction results. We report the mean (\pm SD.) averaged over 10 experiments. D-calibration reports the number of experiments in which the respective model was D-calibrated. To improve readability, we have multiplied the CI and IBS results by 100.

6.3 Multi-event prediction

We now consider the multi-event case ($K > 1$), where the K events are not mutually-exclusive and more than one event can happen per instance. We evaluate MENSA and state-of-the-art baselines in the MIMIC-IV, Rotterdam, PRO-ACT and EBMT test sets. Table 5 shows the prediction results. Overall, MENSA has the best (highest) global local concordance index in the Rotterdam and PRO-ACT datasets, and the best (highest) local concordance index in the MIMIC-IV, Rotterdam and PRO-ACT datasets. This shows a clear advantage in the proposed joint optimization strategy in MENSA, whereas the rival models, except the Hierarchical model, learn a separate model for each event and thus cannot leverage any shared information. MENSA also generally give accurate predictions of the survival function in terms of the integrated Brier Score, and accurate time-to-event estimates in terms of the margin MAE.

Specifically, in the MIMIC-IV dataset, MENSA has the best (highest) local concordance index, the best (lowest) integrated Brier Score, the second-best (second-lowest) margin MAE. Moreover, as we saw in the single-event experiment, MENSA does not sacrifice discriminative performance to achieve calibration in this dataset, as both concordance index and calibration results are solid. In the Rotterdam dataset, MENSA has the best (highest) global and local concordance indices and the best (lowest) margin MAE, while being D-calibrated in 17 of 20 experiments. Although the Rotterdam dataset is considerably smaller than the MIMIC-IV, the performance is still solid and MENSA displays clear strengths over the rival methods. Similarly in PRO-ACT, MENSA has the best (highest) global and local concordance indices, the second-best (second-lowest) margin MAE, and is D-calibrated in 39 of 40 experiments. Lastly, in the EBMT dataset, MENSA has the second-best (second-highest) global and local concordance indices and the second-best (second-lowest) margin MAE. Although MENSA’s predicted survival curves are not well-calibrated in this dataset (7/50), this is probably due to the smaller sample size and the higher number of events compared to other datasets, *e.g.*, MIMIC-IV and Rotterdam.

Dataset	Model	Global CI \uparrow	Local CI \uparrow	IBS \downarrow	mMAE \downarrow	D-Cal \uparrow
MIMIC-IV ($N = 24, 516$, $K = 3, d = 100$)	DeepSurv	71.66\pm0.59	90.12 \pm 0.58	15.02 \pm 1.87	8.93 \pm 1.68	30/30
	DeepHit	70.08 \pm 0.37	89.91 \pm 0.63	16.65 \pm 1.93	8.70\pm1.61	10/30
	Hierarch.	65.82 \pm 1.43	88.50 \pm 1.26	51.04 \pm 13.77	22.82 \pm 6.84	0/30
	MTLR	67.96 \pm 0.33	80.96 \pm 1.44	15.98 \pm 1.75	20.64 \pm 11.03	0/30
	DSM	71.64 \pm 0.64	90.09 \pm 1.01	15.39 \pm 2.10	71.80 \pm 1.72	28/30
	MENSA (Ours)	71.52 \pm 0.47	90.68\pm0.36	12.96\pm2.74	11.13 \pm 1.47	30/30
Rotterdam ($N = 2, 982$, $K = 2, d = 10$)	DeepSurv	69.76 \pm 1.18	81.63 \pm 2.76	19.30 \pm 0.18	22.92 \pm 2.60	18/20
	DeepHit	67.62 \pm 1.13	88.08 \pm 1.71	21.16 \pm 0.84	27.21 \pm 2.43	8/20
	Hierarch.	67.00 \pm 1.45	58.93 \pm 3.27	56.02 \pm 5.57	43.50 \pm 1.56	0/20
	MTLR	70.01 \pm 1.20	83.08 \pm 3.10	18.23\pm0.12	23.06 \pm 2.46	20/20
	DSM	68.31 \pm 1.80	88.53 \pm 3.56	19.33 \pm 0.00	24.03 \pm 3.28	11/20
	MENSA (Ours)	69.94\pm1.38	88.70\pm4.17	20.36 \pm 2.17	18.91\pm6.53	17/20
PRO-ACT ($N = 3, 220$, $K = 4, d = 8$)	DeepSurv	69.44 \pm 0.78	73.46 \pm 1.16	16.92 \pm 1.26	130.15 \pm 15.78	37/40
	DeepHit	67.29 \pm 0.78	71.44 \pm 0.87	19.66 \pm 1.61	145.21 \pm 22.39	18/40
	Hierarch.	69.15 \pm 0.73	73.97 \pm 0.50	54.05 \pm 10.11	281.49 \pm 52.69	0/40
	MTLR	70.69 \pm 0.59	75.95 \pm 0.53	16.39 \pm 1.45	127.11\pm14.40	38/40
	DSM	68.71 \pm 0.88	71.30 \pm 1.14	17.66 \pm 1.47	193.91 \pm 46.84	33/40
	MENSA (Ours)	70.74\pm0.59	76.12\pm0.57	21.09 \pm 6.81	129.03 \pm 10.99	39/40
EBMT ($N = 2, 279$, $K = 5, d = 6$)	DeepSurv	55.08\pm0.68	66.34 \pm 0.91	20.34 \pm 2.63	47.06\pm2.53	49/50
	DeepHit	52.54 \pm 1.10	58.72 \pm 2.61	24.57 \pm 2.65	75.18 \pm 17.90	44/50
	Hierarch.	53.93 \pm 1.22	39.56 \pm 0.71	71.85 \pm 8.27	92.25 \pm 25.01	0/50
	MTLR	53.45 \pm 0.97	60.89 \pm 2.33	18.62\pm2.64	68.45 \pm 15.48	50/50
	DSM	53.49 \pm 1.29	68.46\pm0.89	21.62 \pm 3.21	58.64 \pm 7.98	16/50
	MENSA (Ours)	54.06 \pm 2.10	68.27 \pm 0.85	26.19 \pm 8.38	54.64 \pm 22.39	7/50

Table 5: Multi-event prediction results. We report the mean (\pm SD.) averaged over 10 experiments. D-calibration counts the number of experiments in which the respective model was D-calibrated. To improve readability, we have multiplied the CI and IBS results by 100, and divided the mMAE results in MIMIC-IV by 100.

As a practical motivation for the multi-event case, we consider the problem of predicting functional decline in patients suffering from ALS – which is a rapidly progressing motor neuron disease with a medium survival time of 3 to 5 years. However, instead of simply predicting the time to death (Kuan et al., 2023), we use our method to predict the time to functional decline in patients, which in our case consists of four distinct but related events: “Speaking”, “Swallowing”, “Handwriting” and “Walking” (see Section 5.2 and Appendix D for details). Such predictions can enable medical doctors to make informed, personalized decisions by tailoring treatments and interventions to an individual’s predicted trajectory. This is particularly critical in ALS, where timely interventions – *e.g.*, assistive devices, nutritional support, and respiratory care – can greatly improve a patient’s quality of life. With MENSA, we can train a *single* survival model to predict an individual’s disease trajectory as K individual survival distributions (ISDs). Figure 11 shows such ISDs, from baseline ($t = 0$) to 500 days later, for the i -th patient in the PRO-ACT dataset using different numbers of mixture components (Ψ) for each event. When $\Psi = 1$, the curves exhibit proportional hazards between them. When $\Psi > 1$, the curves have more degrees of freedom and can thus model non-proportional hazards in this scenario. However, this also increases the number of parameters for each event, which comes with some pitfalls – *e.g.*, the risk of overfitting and additional computational costs.

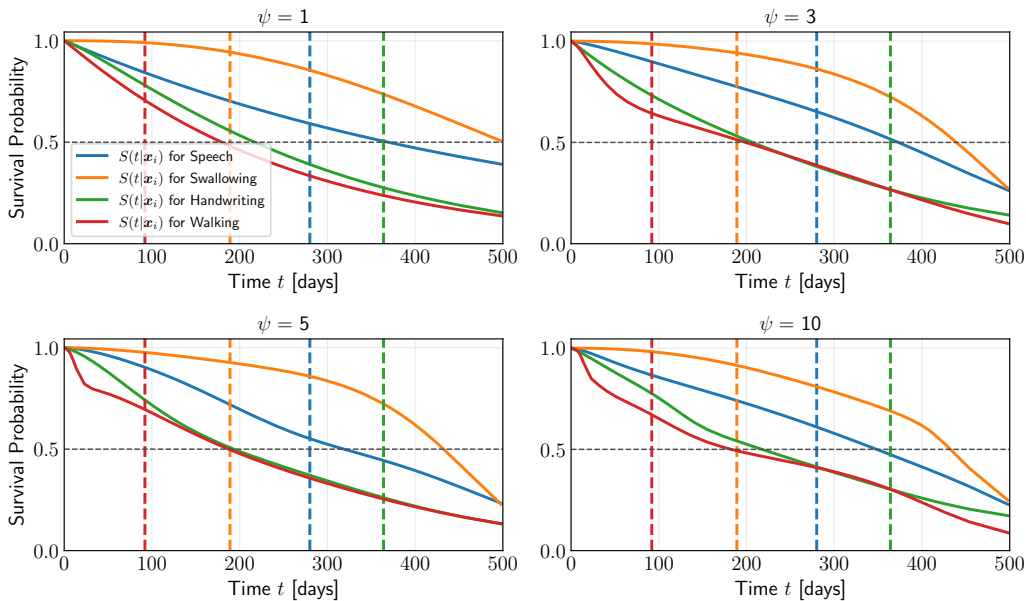


Figure 11: Predicted individual survival distributions (ISDs) for the i -th patient in the PRO-ACT test set using MENSA with different number of mixture components. The point where the survival curve intersects the dashed horizontal line at 50% indicates the predicted time of event. The dashed vertical lines represent patient i 's actual event times for the corresponding events.

6.4 Model complexity

Model	Single-event	Competing risks	Multi-event
DeepSurv	$\mathcal{O}(d)$	$K\mathcal{O}(d)$	$K\mathcal{O}(d)$
DeepHit	$\mathcal{O}(Bd)$	$\mathcal{O}(KBd)$	$K\mathcal{O}(Bd)$
MTLR	$\mathcal{O}(Bd)$	$\mathcal{O}(KBd)$	$K\mathcal{O}(Bd)$
DSM	$\mathcal{O}(\Psi + d)$	$\mathcal{O}(K\Psi + d)$	$K\mathcal{O}(\Psi + d)$
Hierarch.	$\mathcal{O}(MB + d)$	$\mathcal{O}(MKB + d)$	$\mathcal{O}(MKB + d)$
MENSA (Ours)	$\mathcal{O}(P\Psi + d)$	$\mathcal{O}(P\Psi + d)$	$\mathcal{O}(P\Psi + d)$

Table 6: Comparison between the proposed model and state-of-the-art baselines in terms of space complexity. d : number of features, K : number of events, B : number of discrete time bins, M : levels of granularity, Ψ : number of mixture distributions, P : number of states.

Table 6 compares the baseline models and MENSA in terms of space complexity. We make our analyses in the single-event, competing-risks and multi-event scenarios. For a fair comparison, we configure all neural network models with a single hidden layer with 32 nodes. By nature of design, models that cannot learn events jointly have to be trained K times in the multi-event scenario. In this case, the DeepSurv model has a $K\mathcal{O}(d)$ space complexity, where d is the number of features, assuming training is not done in parallel. This can lead to significant increases in the number of trainable parameters in high-dimensional datasets with many events, making it a less-attractive solution. MENSA does not suffer from this problem, as it can train on multiple events at once with a space complexity of $\mathcal{O}(\Psi P + d)$.

Deep learning survival models are usually applied for high-dimensional tasks, where the number of input parameters is large, so parameter and memory efficiency becomes important in such cases. We thus compare our model to rival baselines in terms of the number of trainable parameters and the number of floating-point operations per second (FLOPs) as a function of the number of features. Figure 12 presents the empirical results in single-event, competing-risks and multi-event scenarios. The number of FLOPs is calculated using the “fvcore” library². In the single-event case, MENSA has a slower increase in parameters and FLOPs as the number of covariates increases. It is similar to other models like DSM and DeepSurv in terms of the rate of increase, but requires fewer parameters than DeepHit and MTLR. In competing risks, both the DSM and MENSA models exhibit relatively slow growth in terms of parameters and FLOPs, making them computationally-efficient for large datasets (more than 100 features). Lastly, in the multi-event case, models that cannot learn events jointly have to be trained a total of K times to make predictions for K events (see Table 6). In this case, the number of parameters and FLOPs in MENSA grow more steadily, compared to other models, like DeepSurv or DeepHit, and the growth rate does not accelerate drastically, like in the Hierarchical model. Based on these observations, MENSA is more computationally-efficient in terms of the number of parameters and the number of TFLOPs relative to other models, *e.g.*, Hierarchical, DeepSurv and MTLR. This is further exemplified in multi-event scenarios, which in many instances require a per-event model to be trained.

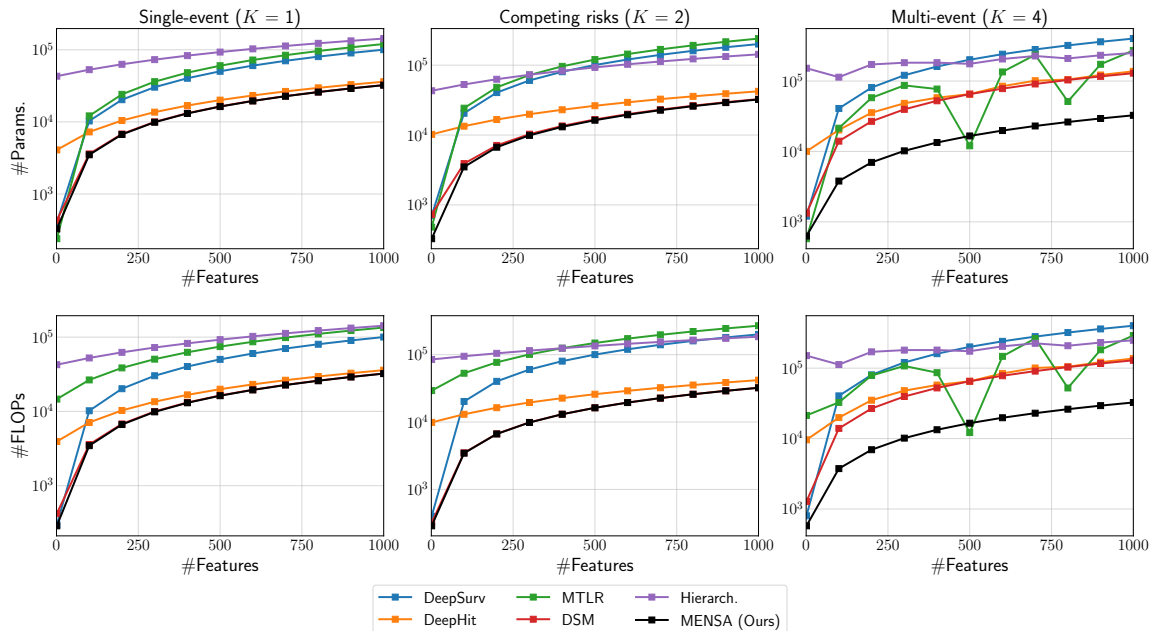


Figure 12: Number of features vs. number of trainable parameters (upper row) and number of floating-point operations (lower row) for single-event ($K = 1$), competing-risks ($K = 2$) and multi-event ($K = 4$) scenarios.

2. Meta Research’s fvcore library, available at <https://github.com/facebookresearch/fvcore> (December 8, 2024).

7 Ablation studies

7.1 Shared feature layer

We perform an ablation study to validate the effectiveness of the proposed shared feature layer in MENSA, $\Phi(x)$. The shared layer takes as input the features $\mathbf{x}^{(i)}$ and outputs a vector, $\tilde{\mathbf{x}}^{(i)}$, that captures the latent representation that is common to the events. Presumably, this allows the model to leverage shared information among the events, and shared feature layers have previously been used in competing-risks and multi-event works (Lee et al., 2018; Kim et al., 2021; Tjandra et al., 2021). We first train MENSA with a shared feature layer across all events, followed by training it with a separate feature layer specific to each event. Table 7 presents the results. In the PRO-ACT dataset, a shared layer gives small improvements in the global concordance index (70.74 vs. 70.68), but a small degradation in the local concordance index (76.12 vs. 76.36). This is possibly due to the lack of conditional dependencies in the PRO-ACT dataset. In the Rotterdam dataset, we see a minor improvement in margin MAE (18.91 vs. 18.71) using a shared layer and a notable improvement in the local concordance index (88.70 vs. 87.96).

Dataset	$\Phi(x)$	Global CI \uparrow	Local CI \uparrow	IBS \downarrow	mMAE \downarrow	D-Cal \uparrow
PRO-ACT	With	70.74 \pm 0.59	76.12 \pm 0.57	21.09 \pm 6.81	129.03 \pm 10.99	39/40
	Without	70.62 \pm 0.58 (-0.18)	76.36 \pm 0.76 (+0.32)	21.02 \pm 6.73 (-0.34)	129.03 \pm 10.96 (0.0)	39/40
Rotterdam	With	69.94 \pm 1.38	88.70 \pm 4.17	20.36 \pm 2.17	18.91 \pm 6.53	17/20
	Without	70.24 \pm 1.25 (+0.42)	87.96 \pm 3.35 (-0.83)	20.34 \pm 2.15 (-0.11)	18.71 \pm 6.22 (-1.1)	18/20

Table 7: Ablation study results for the shared layer on the PRO-ACT and Rotterdam test sets, averaged over 10 experiments with relative improvement/degradation compared to the baseline. D-calibration counts the number of experiments in which the model was D-calibrated. To improve readability, we have multiplied the CI and IBS results by 100 and divided the mMAE results in the Rotterdam dataset by 100.

7.2 Trajectory-based likelihood

We perform an ablation study to measure the effectiveness of the proposed trajectory-based likelihood. This likelihood accounts for known event orderings (*e.g.*, illness must occur before death), and thus encourages the model to predict a high survival probability of a later event at the time an earlier event occurs. In order to determine if the trajectory likelihood improves discrimination or prediction performances, we first train MENSA with this trajectory likelihood, and subsequently without it. Table 8 shows the prediction results in two multi-event datasets. In the Rotterdam dataset, using the trajectory likelihood leads to a small degradation in the global (69.94 vs. 70.08) and local (88.70 vs. 88.76) concordance indices but an improvement in the integrated Brier Score (20.36 vs. 20.54) and the margin MAE (18.91 vs. 18.93). We see the same tendency in the EMBT dataset, as the trajectory likelihood evidently decreases the global concordance index (54.06 vs. 54.13), but improves the local variant (68.27 vs. 68.00), the integrated Brier Score (26.19 vs. 26.32) and the margin MAE (54.64 vs. 55.29). Overall, the trajectory likelihood seems to slightly decrease the discrimination and calibration performances but improve the accuracy of the predicted survival curves and the time-to-event estimates.

Dataset	$\mathcal{L}_{trajectory}$	Global CI \uparrow	Local CI \uparrow	IBS \downarrow	mMAE \downarrow	D-Cal \uparrow
Rotterdam	With	69.94 \pm 1.38	88.70 \pm 4.17	20.36 \pm 2.17	18.91 \pm 6.53	17/20
	Without	70.08 \pm 1.40 (+0.19)	88.76 \pm 3.86 (+0.07)	20.54 \pm 2.36 (+0.92)	18.93 \pm 6.56 (+0.06)	18/20
EBMT	With	54.06 \pm 2.10	68.27 \pm 0.85	26.19 \pm 8.38	54.64 \pm 22.39	7/50
	Without	54.13 \pm 1.76 (+0.14)	68.00 \pm 0.83 (-0.4)	26.32 \pm 8.30 (+0.51)	55.29 \pm 22.99 (+1.18)	10/50

Table 8: Ablation study results for the trajectory-based likelihood on the Rotterdam and EBMT test sets, averaged over 10 experiments with relative improvement/degradation compared to the baseline. D-calibration counts the number of experiments in which the model was D-calibrated. To improve readability, we have multiplied the CI and IBS results by 100 and divided the mMAE results by 100.

8 Discussion

Limitations. One limitation to the present work is that the proposed method assumes conditional independent censoring, *i.e.*, the event time is independent of the censoring time, given the patient’s features ($\mathbf{x}^{(i)}$). In other words, it assumes that any relationship between event and censoring times is captured in the features. However, this assumption may fail to fully account for the dependency if important covariates are missing in the analysis. To this end, we evaluated MENSA under dependent censoring in the single-event case and measured its prediction bias using the Survival- ℓ_1 , *i.e.*, the difference between the predicted survival curve and the true survival curve. We found that the bias was steady in the linear case under dependence from a Frank or Clayton copula, and well-below established baselines, but increased as a function of Kendall’s τ in the nonlinear case, more aligned with the baselines. This shows that MENSA does make biased survival predictions in the nonlinear case in the presence of dependent censoring, although the incurred prediction bias was lower in MENSA than in several rival models.

Another limitation, based on our observations, is that parametric survival models, such as MENSA, often require more data to train effectively and achieve good results compared to semiparametric models, such as Cox-based regression models. These models make fewer assumptions about the underlying survival time distribution, as they only model the hazard function’s proportionality using *e.g.*, the exponential distribution, and leave the baseline hazard unspecified. This makes the CoxPH model and Cox-based models, *e.g.*, CoxBoost and DeepSurv, less sensitive to the dataset’s size and distribution assumptions. On the other hand, parametric models, *e.g.*, DSM and MENSA, assume a specific distribution (*e.g.*, Weibull, exponential) for the survival times. The flexibility of the model can lead to better performance if the parametric assumption is correct and data is plentiful, but it also adds more parameters that need to be estimated.

Future work. The next natural step in our work is to address the aforementioned prediction bias under dependent censoring, as we demonstrated on the synthetic dataset in the single-event case. All survival models in this work, both the established baselines and MENSA, assume conditional independent censoring, and thus may give biased parameter estimates when dependent censoring is present (Emura and Chen, 2018, Ch. 3). Although we can reduce dependent censoring simply by collecting more training data (*i.e.*, features) (Emura and Chen, 2018, Ch. 1), ethical or practical constraints in medical studies may prevent us from doing so, especially in large-scale or long-term studies. Alternatively,

we can incorporate the dependence between event distributions outside the features in the parameter estimation by learning it as a function of the data: Foomani et al. (2023) proposed learning a survival model under dependent censoring by modifying the survival likelihood in Equation 1 to include a copula from the Archimedean family (*e.g.*, Clayton, Frank). Although a detailed discussion is beyond the scope of this work, this copula-dependent likelihood is split into four terms: the first two terms account for the log-likelihood of observing an event and its conditional probability given the copula, while the last two terms do the same for the censoring. The copula’s partial derivatives have closed-form solutions for Archimedean copulas, which enable efficient optimization using gradient-based methods in MLE. This approach can be extended to a multi-event scenario by first estimating a K -variate copula model for the joint event distribution and then incorporate the model into the survival likelihood across K events.

An alternative approach is to parameterize the copula as a neural network, which eliminates the need to specify the copula family – *e.g.*, Clayton or Frank – beforehand. Recent studies have adopted this approach and shown promising results for single-event (Zhang et al., 2024) and competing-risks (Liu et al., 2024) scenarios. Zhang et al. (2024) proposed DCSurvival, an end-to-end framework that estimates the survival marginals using monotonic neural density estimators (NDE) and parameterizes the (Archimedean) copula generator function as a neural network, φ_{nn} . Unlike Foomani et al. (2023), DCSurvival does not make assumptions about the copula family, other than that it is Archimedean, since it learns the copula nonparametrically. However, using a single Archimedean copula can characterize only a symmetric dependency relationship. To this end, Liu et al. (2024) proposed HACSurv, which extends DCSurvival to competing risks by modeling $C(u_0, \dots, u_K)$ using a flexible hierarchical Archimedean copula (HAC). Thus, this model can capture diverse forms of dependencies between competing events. An open avenue for future research is to extend these hierarchical copulas to the multi-event setting.

Boarder impacts. This paper proposes a new method for survival analysis, where there are multiple events of interest, accompanied by experiments on five publicly-available clinical datasets to show the practical usefulness of the model. These datasets were used following the guidance of the respective data providers and domain experts. We acknowledge that survival analysis can give valuable insights in treatment planning or personalized care, but can also have adverse impacts if misinterpreted or misused, or if the dataset contains systemic biases, leading to inequities or discrimination. The deployment of such models comes with several potential risks: (1) If the training data is not representative of the population and subgroups the models are used within, they may disproportionately favor certain groups over others. (2) Covariate-based survival models, similar to other machine learning models, can unintentionally use sensitive variables (*e.g.*, race, gender, or socioeconomic status), which can lead to biased predictions. (3) Survival models can replace human decision-makers in certain domains, such as healthcare, and autonomously decide who gets access to treatment and who does not based on some criteria. This, again, may reproduce or amplify existing biases in the data, leading to unfair or discriminatory results. To mitigate these risks, we emphasize the importance of adequate evaluation and testing before deploying such models, and that these models should be used as a decision-support tool in the healthcare section rather than as an independent oracle for decision-making.

9 Conclusion

We have presented MENSA, a novel method for multi-event survival analysis. Given an instance, the model predicts the time until that instance experiences each of several different events, including being event-free. In real clinical datasets, we show that the proposed method led to improvements over well-accepted baselines in several performance metrics, especially in terms of predictive accuracy (Brier Score and MAE), local discrimination (*i.e.*, ranking of events within individuals) and distribution calibration. An ablation study showed that combining the traditional log-likelihood in multi-event with a trajectory-based likelihood, which promotes learning temporal patterns between events, consistently improved the Brier Score and MAE in two multi-event datasets. We also highlighted the advantages that our model holds over state-of-the-art baselines in terms of computational efficiency and resource utilization, especially in the multi-event scenario, where traditional survival models need to train a model for each event. As a practical motivation for the multi-event case, we predicted the time to functional decline in ALS patients, which in our case consisted of four separate, but related events. This application can facilitate the design of personalized treatment plans for the disease and improve a patient’s quality of life.

Acknowledgments

This research received support from the Natural Science and Engineering Research Council of Canada (NSERC), the Canadian Institute for Advanced Research (CIFAR), and the Alberta Machine Intelligence Institute (Amii).

†Data used in the preparation of this article were obtained from the Pooled Resource Open-Access ALS Clinical Trials (PRO-ACT) Database. As such, the following organizations and individuals within the PRO-ACT Consortium contributed to the design and implementation of the PRO-ACT Database and/or provided data, but did not participate in the analysis of the data or the writing of this report: ALS Therapy Alliance, Cytokinetics, Inc., Amylyx Pharmaceuticals, Inc., Knopp Biosciences, Neuraltus Pharmaceuticals, Inc., Neurological Clinical Research Institute, MGH, Northeast ALS Consortium, Novartis, Orion Corporation, Prize4Life Israel, Regeneron Pharmaceuticals, Inc., Sanofi, Teva Pharmaceutical Industries, Ltd., The ALS Association.

References

- Odd Aalen. Nonparametric Inference for a Family of Counting Processes. *The Annals of Statistics*, 6(4):701–726, 1978.
- Per K. Andersen and Niels Keiding. Multi-state models for event history analysis. *Statistical Methods in Medical Research*, 11(2):91–115, 2002.
- Gregory T. Armstrong, Toana Kawashima, Wendy Leisenring, Kayla Stratton, Marilyn Stovall, Melissa M. Hudson, Charles A. Sklar, Leslie L. Robison, and Kevin C. Oeffinger. Aging and risk of severe, disabling, life-threatening, and fatal events in the childhood cancer survivor study. *Journal of Clinical Oncology*, 32(12):1218, 2014.

- Nazem Atassi, James Berry, Amy Shui, Neta Zach, Alexander Sherman, Ervin Sinani, Jason Walker, Igor Katsovskiy, David Schoenfeld, Merit Cudkowicz, and Melanie Leitner. The PRO-ACT database: design, initial analyses, and predictive features. *Neurology*, 83(19):1719–1725, 2014.
- George H. Chen. An Introduction to Deep Survival Analysis Models for Predicting Time-to-Event Outcomes. *Foundations and Trends in Machine Learning*, 17(6):921–1100, 2024.
- David R. Cox. Regression models and life-tables. *Journal of the Royal Statistical Society: Series B (Methodological)*, 34(2):187–202, 1972.
- Cameron Davidson-Pilon. lifelines: survival analysis in Python. *Journal of Open Source Software*, 4(40):1317, 2019.
- Takeshi Emura and Yi-Hau Chen. *Analysis of Survival Data with Dependent Censoring: Copula-Based Approaches*. Springer, 2018.
- David Faraggi and Richard Simon. A Neural Network Model for Survival Data. *Statistics in Medicine*, 14:73–82, 1995.
- Evelyn Fix and Jerzy Neyman. A Simple Stochastic Model of Recovery, Relapse, Death and Loss of Patients. *Human Biology*, 23(3):205–241, Sep 1951.
- Ali H. G. Foomani, Michael Cooper, Russell Greiner, and Rahul G. Krishnan. Copula-based deep survival models for dependent censoring. In *Proceedings of the 39th Conference on Uncertainty in Artificial Intelligence*, volume 216, pages 669–680, 2023.
- James Gareth, Witten Daniela, Hastie Trevor, and Tibshirani Robert. *An introduction to statistical learning: with applications in R*. Springer, 2 edition, 2021.
- Erika Graf, Claudia Schmoor, Willi Sauerbrei, and Martin Schumacher. Assessment and comparison of prognostic classification schemes for survival data. *Statistics in medicine*, 18(17-18):2529–2545, 1999.
- Mehak Gupta, Brennan Gallamoza, Nicolas Cutrona, Pranjali Dhakal, Raphael Poulain, and Rahmatollah Beheshti. An Extensive Data Processing Pipeline for MIMIC-IV. In *Proceedings of the 2nd Machine Learning for Health symposium*, volume 193, pages 311–325, 2022.
- Humza Haider, Bret Hoehn, Sarah Davis, and Russell Greiner. Effective Ways to Build and Evaluate Individual Survival Distributions. *Journal of Machine Learning Research*, 21(1):1–63, 2020.
- Frank E. Harrell Jr., Robert M. Califf, David B. Pryor, Kerry L. Lee, and Robert A. Rosati. Evaluating the Yield of Medical Tests. *JAMA*, 247(18):2543–2546, 1982.
- Jin-Jian Hsieh and Jian-Lin Wang. Quantile residual life regression based on semi-competing risks data. *Journal of Applied Statistics*, 45(10):1770–1780, 2018.
- Hemant Ishwaran, Udaya B. Kogalur, Eugene H. Blackstone, and Michael S. Lauer. Random Survival Forests. *The Annals of Applied Statistics*, 2(3):841–860, 2008.

- Fei Jiang and Sebastien Haneuse. A semi-parametric transformation frailty model for semi-competing risks survival data. *Scandinavian Journal of Statistics*, 44(1):112–129, 2017.
- Alistair E. W. Johnson, Lucas Bulgarelli, Lu Shen, Alvin Gayles, Ayad Shammout, Steven Horng, Tom J. Pollard, Sicheng Hao, Benjamin Moody, Brian Gow, Li wei H. Lehman, Leo A. Celi, and Roger G. Mark. MIMIC-IV, a freely accessible electronic health record dataset. *Scientific Data*, 10(1):1–9, 2023.
- Edwin L. Kaplan and Paul Meier. Nonparametric Estimation from Incomplete Observations. *Journal of the American Statistical Association*, 53(282):457–481, 1958.
- Jared Katzman, Uri Shaham, Jonathan Bates, Alexander Cloninger, Tingting Jiang, and Yuval Kluger. DeepSurv: personalized treatment recommender system using a Cox proportional hazards deep neural network. *BMC Medical Research Methodology*, 18(1):1–12, 2018.
- Sejin Kim, Michal Kazmierski, and Benjamin Haibe-Kains. Deep-CR MTLR: a Multi-Modal Approach for Cancer Survival Prediction with Competing Risks. In *Proceedings of AAAI Spring Symposium on Survival Prediction - Algorithms, Challenges, and Applications*, volume 146, pages 223–231, 2021.
- Diederik P. Kingma and Jimmy Ba. Adam: A Method for Stochastic Optimization, 2017. URL <https://arxiv.org/abs/1412.6980>.
- Günter Klambauer, Thomas Unterthiner, and Andreas Mayr. Self-Normalizing Neural Networks. In *Advances in Neural Information Processing Systems*, volume 30, pages 972–981, 2017.
- John P. Klein and Melvin L. Moeschberger. *Survival analysis: techniques for censored and truncated data*. Springer Science & Business Media, 2006.
- Li-Hao Kuan, Pedram Parnianpour, Rafsanjany Kushol, Neeraj Kumar, Tanushka Anand, Sanjay Kalra, and Russell Greiner. Accurate personalized survival prediction for amyotrophic lateral sclerosis patients. *Scientific Reports*, 13(1):20713, 2023.
- Martin G. Larson. Covariate Analysis of Competing-Risks Data with Log-Linear Models. *Biometrics*, 40(2):459–469, 1984.
- Changhee Lee, William Zame, Jinsung Yoon, and Mihaela van der Schaar. DeepHit: A Deep Learning Approach to Survival Analysis With Competing Risks. *Proceedings of the AAAI Conference on Artificial Intelligence*, 32(1):1145–1152, Apr. 2018.
- Yan Li, Jie Wang, Jieping Ye, and Chandan K. Reddy. A Multi-Task Learning Formulation for Survival Analysis. In *Proceedings of the 22nd ACM SIGKDD International Conference on Knowledge Discovery and Data Mining*, page 1715–1724, 2016.
- Christian M. Lillelund, Michael Harbo, and Christian F. Pedersen. Prognosis of fall risk in home care clients: A noninvasive approach using survival analysis. *Journal of Public Health*, pages 1–13, 2024a.

- Christian M. Lillelund, Martin Magris, and Christian F. Pedersen. Efficient Training of Probabilistic Neural Networks for Survival Analysis. *IEEE Journal of Biomedical and Health Informatics*, pages 1–10, 2024b.
- Xin Liu, Weijia Zhang, and Min-Ling Zhang. HACSurv: A Hierarchical Copula-based Approach for Survival Analysis with Dependent Competing Risks. *arXiv preprint arXiv:2410.15180*, 2024.
- Hans C. van Houwelingen Marta Fiocco, Hein Putter. Reduced-rank proportional hazards regression and simulation-based prediction for multi-state models. *Statistics in Medicine*, 27:4340–4358, 2008.
- Chirag Nagpal, Xinyu Li, and Artur Dubrawski. Deep Survival Machines: Fully Parametric Survival Regression and Representation Learning for Censored Data with Competing Risks. *IEEE Journal of Biomedical and Health Informatics*, 25(8):3163–3175, 2021.
- Wayne Nelson. Hazard Plotting for Incomplete Failure Data. *Journal of Quality Technology*, 1:27–52, 1969.
- Ross L. Prentice and John D. Kalbfleisch. Hazard rate models with covariates. *Biometrics*, pages 25–39, 1979.
- Shi-ang Qi, Neeraj Kumar, Jian-Yi Xu, Jaykumar Patel, Sambasivarao Damaraju, Grace Shen-Tu, and Russell Greiner. Personalized breast cancer onset prediction from lifestyle and health history information. *Plos one*, 17(12):e0279174, 2022.
- Shi-ang Qi, Neeraj Kumar, Mahtab Farrokh, Weijie Sun, Li Hao Kuan, Rajesh Ranganath, Ricardo Henao, and Russell Greiner. An Effective Meaningful Way to Evaluate Survival Models. In *Proceedings of the 40th International Conference on Machine Learning*, volume 202, pages 28244–28276, 2023a.
- Shi-ang Qi, Weijie Sun, and Russell Greiner. SurvivalEVAL: A Comprehensive Open-Source Python Package for Evaluating Individual Survival Distributions. In *Proceedings of the 2023 AAAI Fall Symposia*, volume 2, pages 453–457, 2023b.
- Greg Ridgeway. The State of Boosting. *Computing Science and Statistics*, 31:172–181, 1999.
- Lynn A. Gloeckler Ries, Marsha E. Reichman, Denise Riedel Lewis, Benjamin F. Hankey, and Brenda K. Edwards. Cancer survival and incidence from the Surveillance, Epidemiology, and End Results (SEER) program. *Oncologist*, 8(6):541–552, 2003.
- Hagai Rossman, Ayya Keshet, and Malka Gorfine. PyMSM: Python package for Competing Risks and Multi-State models for Survival Data. *Journal of Open Source Software*, 7(78):4566, 2022.
- Patrick Royston and Douglas G. Altman. External validation of a Cox prognostic model: principles and methods. *BMC Medical Research Methodology*, 13:33, 2013.

- Konstantinos Sechidis, Grigorios Tsoumakas, and Ioannis Vlahavas. On the Stratification of Multi-label Data. In *Proceedings of the Joint European Conference on Machine Learning and Knowledge Discovery in Databases*, pages 145–158, 2011.
- Richard M. Simon, Edward L. Korn, Lisa M. McShane, Michael D. Radmacher, George W. Wright, and Yingdong Zhao. *Design and analysis of DNA microarray investigations*, volume 209. Springer, 2003.
- Jasper Snoek, Hugo Larochelle, and Ryan P. Adams. Practical Bayesian Optimization of Machine Learning Algorithms. In *Advances in Neural Information Processing Systems*, volume 25, pages 2951–2959, 2012.
- Scott D. Solomon, Adel R. Rizkala, Jianjian Gong, Wenyan Wang, Inder S. Anand, Junbo Ge, Carolyn S. P. Lam, Aldo P. Maggioni, Felipe Martinez, Milton Packer, Marc A. Pfeffer, Burkert Pieske, Margaret M. Redfield, Jean L. Rouleau, Dirk J. Van Veldhuisen, Faiez Zannad, Michael R. Zile, Akshay S. Desai, Victor C. Shi, Martin P. Lefkowitz, and John J. V. McMurray. Angiotensin receptor neprilysin inhibition in heart failure with preserved ejection fraction: rationale and design of the PARAGON-HF trial. *JACC: Heart Failure*, 5(7):471–482, 2017.
- Erling Sverdrup. Estimates and Test Procedures in Connection with Stochastic Models for Deaths, Recoveries and Transfers Between Different States of Health. *Scandinavian Actuarial Journal*, 1965(3-4):184–211, 1965.
- Donna Tjandra, Yifei He, and Jenna Wiens. A Hierarchical Approach to Multi-Event Survival Analysis. *Proceedings of the AAAI Conference on Artificial Intelligence*, 35(1):591–599, 2021.
- Anastasios Tsiatis. A Nonidentifiability Aspect of the Problem of Competing Risks. *Proceedings of the National Academy of Sciences of the United States of America*, 72(1):20–22, 1975.
- Lu Wang, Yan Li, Jiayu Zhou, Dongxiao Zhu, and Jieping Ye. Multi-task Survival Analysis. In *2017 IEEE International Conference on Data Mining (ICDM)*, pages 485–494, 2017.
- Zifeng Wang and Jimeng Sun. SurvTRACE: Transformers for Survival Analysis with Competing Events. In *Proceedings of the 13th ACM International Conference on Bioinformatics, Computational Biology and Health Informatics*, 2022.
- Chun-Nam Yu, Russell Greiner, Hsiu-Chin Lin, and Vickie Baracos. Learning Patient-Specific Cancer Survival Distributions as a Sequence of Dependent Regressors. In *Advances in Neural Information Processing Systems*, volume 24, pages 1845–1853, 2011.
- Weijia Zhang, Chun Kai Ling, and Xuanhui Zhang. Deep Copula-Based Survival Analysis for Dependent Censoring with Identifiability Guarantees. In *Proceedings of the AAAI Conference on Artificial Intelligence*, volume 38, pages 20613–20621, 2024.

Appendix A. Notation

Table 9 provides a list of notations used in this work.

Symbol	Definition
$c_k^{(i)}$	Censoring time of observation i for event k
$e_k^{(i)}$	Event time of observation i for event k
$t_k^{(i)}$	Observed time of observation i for event k
$\delta_k^{(i)}$	Event indicator, $\delta_k^{(i)} = 1_{e_k^{(i)} > c_k^{(i)}}$
\mathcal{D}	Raw survival dataset
N	Number of observations in the dataset
d	Number of features/covariates in the dataset
$\mathbf{x}^{(i)}$	Covariates of observation i
$h_0(t)$	Baseline hazard function
$h(\cdot \mathbf{x}^{(i)})$	Hazard function given the covariates $\mathbf{x}^{(i)}$
$G(t) \in \mathcal{S}$	A Markov process with state space \mathcal{P}
$K \in \mathcal{K}$	Number of events, and space of events
$\mathcal{T} \in \mathcal{K}$	Trajectory set over the space of events
$P \in \mathcal{P}$	Number of states, and space of states
\mathcal{L}	Objective/likelihood function
L	Number of training epochs
λ	Learning rate
Ψ	Number of mixture distributions
$f(\boldsymbol{\theta}, \mathbf{x}^{(i)})$	Risk function given model parameters and features
S_T	Survival function, $S : \mathbb{R} \rightarrow [0, 1]$
f_T	Probability density function, representing $\Pr(T = t)$
F_T	Cumulative density function, representing $\Pr(T < t)$
C_θ	A copula parameterized by θ
u_1, u_2	Inputs to a copula function

Table 9: Table of notation.

Appendix B. Evaluation metrics

Harrell’s CI: The concordance index (CI) measures the discriminative performance of a survival model by calculating the proportion of concordant pairs among all comparable pairs. A pair is considered comparable if we can determine who has the event first. It is defined as (Harrell Jr. et al., 1982):

$$\text{CI} = \frac{\sum_{i,j \in \mathcal{D}} \mathbb{1}_{t^{(i)} < t_j} \cdot \mathbb{1}_{\eta^{(i)} > \eta_j} \cdot \delta^{(i)}}{\sum_{i,j \in \mathcal{D}} \mathbb{1}_{t^{(i)} < t_j} \cdot \delta^{(i)}}, \quad (9)$$

where $\eta^{(i)}$ and $\eta^{(j)}$ represent risk scores for individuals i and j , respectively.

Global CI: The global CI is calculated as the average of the CI values across all specific events, providing an overall measure of a model’s discriminative performance for all

competing and multiple events. This approach follows previous work (Lee et al., 2018; Katzman et al., 2018), ensuring a comprehensive evaluation of the model’s global discrimination ability. It is defined as:

$$\text{Global CI} = \frac{\sum_{k \in \mathcal{K}} \sum_{i, j \in \mathcal{D}_k} \mathbb{1}_{t^{(i)} < t_j} \cdot \mathbb{1}_{\eta^{(i)} > \eta_j} \cdot \delta^{(i)}}{\sum_{k \in \mathcal{K}} \sum_{i, j \in \mathcal{D}_k} \mathbb{1}_{t^{(i)} < t_j} \cdot \delta^{(i)}}, \quad (10)$$

where \mathcal{K} represents the set of all distinct events, and the index k corresponds to the k -th specific event.

Local CI: The local CI is computed by averaging CI scores across multiple events for each instance, and was proposed by Tjandra et al. (2021). This metric evaluates the model’s ability to discriminate between multiple events within a single instance. It is defined as (Tjandra et al., 2021):

$$\text{Local CI} = \frac{\sum_{i \in N} \sum_{k_1, k_2 \in \mathcal{K}^{(i)}} \mathbb{1}_{t_{k_1} < t_{k_2}} \cdot \mathbb{1}_{\eta_{k_1} > \eta_{k_2}} \cdot \delta_{k_1}}{\sum_{i \in N} \sum_{k_1, k_2 \in \mathcal{K}^{(i)}} \mathbb{1}_{t_{k_1} < t_{k_2}} \cdot \delta_{k_1}}, \quad (11)$$

where $\mathcal{K}^{(i)}$ represents the set of all K different events for instance i , and η_{k_1} and η_{k_2} denote the risk scores associated with the two events, respectively.

BS/IBS: The Brier Score (BS) is defined as the mean squared difference between the predicted survival curve and the Heaviside step function of the observed event. The integrated Brier Score (Graf et al., 1999) (IBS) aggregates the Brier Scores across multiple time points to provide a single measure of model performance. We use inverse probability weighting (IPCW) to handle censored events. The BS is defined as:

$$\text{BS}(t^*) = \frac{1}{N} \sum_{i \in \mathcal{D}} \left[\frac{S(t^* | \mathbf{x}^{(i)})^2 \cdot \mathbb{1}_{t^{(i)} \leq t^*, \delta^{(i)}=1}}{G(t^{(i)})} + \frac{(1 - S(t^* | \mathbf{x}^{(i)}))^2 \cdot \mathbb{1}_{t^{(i)} > t^*}}{G(t^*)} \right], \quad (12)$$

which is the mean square error between observe survival status and survival probability at time t^* and where $G(t^*)$ is the non-censoring probability at time t^* . The IBS is defined as:

$$\text{IBS} = \frac{1}{N} \sum_{i \in \mathcal{D}} \frac{1}{t_{\max}} \cdot \int_0^{t_{\max}} \text{BS}(t) dt, \quad (13)$$

where t_{\max} is the maximum observed time.

MAE: The mean absolute error (MAE) is the absolute difference between the predicted and actual survival times. Given an individual survival distribution, $S(t | \mathbf{x}_i) = \Pr(T > t | \mathbf{x}_i)$, we calculate the predicted survival time $\hat{t}^{(i)}$ using the median time of the predicted survival distribution (Qi et al., 2023b):

$$\hat{t}^{(i)} = \text{median}(S(t | \mathbf{x}_i)) = S^{-1}(\tau = 0.5 | \mathbf{x}_i), \quad (14)$$

$$\text{MAE}(\hat{t}_i, t_i, \delta_i = 1) = |t_i - \hat{t}_i|. \quad (15)$$

For censored individuals, we calculate the marginal MAE (mMAE), as proposed by Haider et al. (2020):

$$\begin{aligned} \text{mMAE} &= \frac{1}{\sum_{i=1}^N \omega^{(i)}} \sum_{i=1}^N \omega^{(i)} \left| [(1 - \delta^{(i)}) \cdot e_m(t^{(i)}) + \delta^{(i)} \cdot t^{(i)}] - \hat{t}^{(i)} \right|, \\ \text{where } e_m(t^{(i)}) &= \begin{cases} t^{(i)} + \frac{\int_{t^{(i)}}^{\infty} S_{\text{KM}}(t) dt}{S_{\text{KM}}(t)} & \text{if } \delta^{(i)} = 0 \\ t^{(i)} & \text{if } \delta^{(i)} = 1 \end{cases}, \\ \text{and } \omega^{(i)} &= \begin{cases} 1 - S_{\text{KM}}(t^{(i)}) & \text{if } \delta^{(i)} = 0 \\ 1 & \text{if } \delta^{(i)} = 1 \end{cases}. \end{aligned} \quad (16)$$

D-calibration: Distribution Calibration (Haider et al., 2020) measures the calibration performance of $S(t)$, expressing to what extent the predicted probabilities can be trusted. We assess this using a Pearson’s χ^2 goodness-of-fit test. For any probability interval $[a, b] \in [0, 1]$, we define $D_m(a, b)$ as the group of individuals in the dataset D whose predicted probability of event is in the interval $[a, b]$ (Qi et al., 2023a). A model is D-calibrated if the proportion of individuals $|D_m(a, b)|/|D|$ is statistically similar to the amount $b - a$. In the results, we count the number of times a model is D-calibrated (at $p > 0.05$) for each event in 10 experiments.

Survival- ℓ_1 : The Survival- ℓ_1 is the L1 distance between the ground-truth survival curve, $S_{T|X}$, and the estimated survival curve, $\hat{S}_{T|X}$, over the event horizon (Foomani et al., 2023). We normalize the area between the survival curves by $T_{\max}^{(i)} = S_{T|X}^{-1}(Q_{\parallel} \cdot \parallel)$ to ensure that the duration spanned by an instance’s survival curve does not influence that instance’s contribution to the metric relative to other instances. The Survival- ℓ_1 is defined as (Foomani et al., 2023):

$$C_{\text{Survival-}\ell_1}(S, \hat{S}) = \frac{1}{N} \sum_{i=1}^N \frac{1}{T_{\max}^{(i)}} \int_0^{\infty} \left| S_{T|X}(t | X^{(i)}) - \hat{S}_{T|X}(t | X^{(i)}) \right| dt. \quad (17)$$

Appendix C. Dependent censoring and copulas

Dependent censoring is a type of informative censoring where the dependence between the censoring time and the survival time is not explained by any observable covariate (Emura and Chen, 2018, Ch. 1). In other words, dependent censoring is a consequence of some residual dependence – *i.e.*, when covariates influencing both survival time and censoring time are ignored or not included in the analysis. A copula is a function that links R.V.s by specifying their dependence structure (Emura and Chen, 2018, Ch. 1), thus it can be applied to introduce a dependence between the event and the censoring distribution.

Formally, we write $C(u_1, \dots, u_d) : [0, 1]^d \rightarrow [0, 1]$, which is a d -dimensional copula (*i.e.*, where d is the number of variables) with u_1, \dots, u_d uniform marginal probabilities. For simplicity, we assume the single-event case, where T_E is the event time, T_C is the censoring time, \mathbf{x} is a vector of covariates, and $S_{T_E}(t | \mathbf{x}) = \Pr(T_E > t_e | \mathbf{x})$ and $S_{T_C}(u | \mathbf{x}) = \Pr(T_C > t_c | \mathbf{x})$ are the marginal survival functions given \mathbf{x} . We can then define a bivariate survival copula C_θ that describes the degree of dependence between T_E and T_C (Emura and

Chen, 2018, Ch. 3):

$$\Pr(T_E > t_e, T_C > t_c | \mathbf{x}) = C_\theta\{S_{T_E}(t_e | \mathbf{x}), S_{T_C}(t_c | \mathbf{x})\}. \quad (18)$$

If C_θ satisfies certain mathematical conditions, then Eq. (18) is a valid survival function (Emura and Chen, 2018, Ch. 3). Kendall's tau (τ) is a common measure of the dependency between T_E and T_C :

$$\tau = \Pr\{(T_2 - T_1)(C_2 - C_1) \geq 0 | \mathbf{x}\} - \Pr\{(T_2 - T_1)(C_2 - C_1) < 0 | \mathbf{x}\}, \quad (19)$$

where (T_1, C_1) and (T_2, C_2) are sampled from the model (18). An Archimedean copula is defined as (Emura and Chen, 2018, Ch. 3):

$$C_\theta(u, v) = \varphi_\theta^{-1}(\varphi_\theta(u) + \varphi_\theta(v)), \quad (20)$$

where the function $\varphi_\theta : [0, 1] \rightarrow [0, 1]$ is called a generator of the copula, which is continuous and strictly decreasing from $\varphi_\theta(0) \geq 0$ to $\varphi_\theta(1) = 0$. The following Archimedean copulas are used in this work:

- **The Independence copula:** $C(u, v) = uv$.
- **The Clayton copula:**

$$C_\theta(u, v) = \left(u^{-\theta} + v^{-\theta} - 1\right)^{-1/\theta}, \quad \theta \geq 0.$$

- **The Frank copula:**

$$C_\theta(u, v) = -\frac{1}{\theta} \log \left[1 + \frac{(e^{-\theta u} - 1)(e^{-\theta v} - 1)}{e^{-\theta} - 1} \right].$$

$\theta \neq 0.$

Appendix D. Data generation and preprocessing details

Synthetic: This paper utilizes two (linear and nonlinear) synthetic datasets with two competing events (event and censoring), both based on the semiparametric Weibull distribution as discussed in Foomani et al. (2023). The datasets are characterized by the conditional hazard function and conditional survival probability of an event as follows:

$$h_{T|X}(t | X) = \left(\frac{v}{\rho}\right) \left(\frac{t}{\rho}\right)^{v-1} \exp(g_\Psi(X)), \quad (21)$$

$$S_{T|X}(t | X) = \exp\left(-\left(\frac{t}{\rho}\right)^{v-1} \exp(g_\Psi(X))\right), \quad (22)$$

where v and ρ represent the shape and scale parameters of the Weibull distribution, respectively. We use $v_E = 4$, $v_C = 5$, $\rho_E = 18$, $\rho_C = 17$. The function $g_\Psi(X)$ represents

the risk function, which is a linear function for the linear dataset and a single-layer neural network with ReLU activation for the non-linear dataset. The data generation process begins by initializing a copula with a predefined parameter θ . We then sample N sets of CDF observations from the copula, each containing two CDF probabilities (corresponding to each competing event). From these probabilities, we then calculate the corresponding times using the inverse function of (22). This data generation process has been described in Algorithm 2 in Foomani et al. (2023).

SEER: Surveillance, Epidemiology, and End Results (SEER) Program dataset (Ries et al., 2003) is a comprehensive collection of clinical data in the United States. This dataset, which encompasses about 49% of the U.S. population, includes vital information on patient diagnoses, time until an event occurs, and other relevant details sourced from various registries. We use the raw feature “COD to site recode” to extract the event indicator. In particular, we focus on two types of events: breast cancer and heart disease. Then, we apply some special value processing for some features, based on the guideline provided by Wang and Sun (2022). For categorical features, missing values are imputed using the mode, followed by one-hot encoding. The data is then standardized to ensure consistency in our analyses. The SEER cohort is available for download at www.seer.cancer.gov.

MIMIC-IV: We utilized the MIMIC-IV v2.2 dataset (Johnson et al., 2023), which includes data on 299,712 patients and 431,231 admissions. Preprocessing was conducted using the MIMIC-IV Pipeline method (Gupta et al., 2022), through which we extracted 1,672 static features from the dataset. To focus our analysis, we filtered the dataset to include only 26,236 patients aged 60 and 65 years. For feature refinement, we applied the Unixox feature selection method (Qi et al., 2022; Simon et al., 2003). In the training set, we assessed the statistical significance of each feature by calculating the p-values using lifelines’s (Davidson-Pilon, 2019) CoxPHFitter summary. The top 100 features with the smallest p-values were selected. The event of interest in our study is mortality after hospital admission. The final set of features is included in the source code. The MIMIC-IV v2.2 is available for download at <https://physionet.org/content/mimiciv/2.2/>.

Rotterdam: The Rotterdam dataset (Royston and Altman, 2013) consists of records of 2,982 primary breast cancer patients included in the Rotterdam tumor bank, with 1,546 of these patients having node-positive disease. The dataset contains 10 covariates, including demographic information, tumor characteristics, and treatment details. Survival time is defined as the duration from primary surgery to the occurrence of either disease recurrence or death from any cause, representing two competing risks. During preprocessing, categorical size groups (≤ 20 , $20 - 50$, > 50) were converted to their approximate median values (10, 35, 75, respectively). Additionally, the remaining features were normalized to ensure consistency across the dataset. The Rotterdam dataset is available in at <https://rdrr.io/cran/survival/man/rotterdam.html>.

PRO-ACT: The PRO-ACT dataset (Atassi et al., 2014) contains over 11,600 clinical records (October 4 2024) from different ALS trials, including demographic, lab, family history, and medical data. In each trial, patients adhere to a schedule of visitations until the study concludes, they become too ill to continue or decide to leave the study. Covariates are recorded at each visitation, including total ALSFRS-R scores, age, gender, region of onset (*e.g.*, limb or bulbar), mean forced vital capacity (FVC) scores, time since diagnosis in days, disease progression rate, and whether the patient is taking Riluzole. For our

analyses, we only use information about each patient from their baseline visitation. At each visitation in the dataset, that patient’s disease state is evaluated by a clinician using the ALSFRS-R assessment. We consider four events: “Speech”, “Swallowing”, “Handwriting” and “Walking”. We consider an event to have occurred the first time a patient scores 2 or less in that specific assessment during any follow-up visitation following their baseline visitation. These four events can occur in any order and are not mutually exclusive. There are several types of censoring, including death, being unable to perform the assessment or leaving the study prematurely. We use a maximum follow-up time of 500 days to focus on the early stages of the disease. We consider patients that score 2 or less in any of the four assessments at baseline as having already had the event, indicating that the loss of function occurred before trial entry, and exclude patients these from the study. We exclude patients with no recorded ALSFRS-R history. The PRO-ACT dataset is available for download at <https://ncr11.partners.org/ProACT>.

EBMT: The EBMT dataset (Rossman et al., 2022) consists of 2,279 patient records who underwent blood or marrow transplantation between 1985 and 1998. The dataset is provided by the European Society for Blood and Marrow Transplantation (EBMT). The dataset focuses on survival after transplantation for patients suffering from blood cancer. We considered five events in our analysis: “Recovery” (Rec), “Adverse Event” (AE), a combination of both (AE and Rec), “Relapse”, and “Death”. These events allowed us to evaluate their individual and combined effects on patient prognosis. The dataset includes six features belong to four baseline covariates: donor-recipient match (where a gender mismatch is defined as a female donor and a male recipient), prophylaxis type, year of transplant, and age at transplant. The year of transplantation was encoded as Boolean variables indicating whether the transplant took place during 1990-1994 and 1995-1998, and the age at the transplantation was classified into Boolean variables indicating whether the age was ≤ 20 or ≥ 40 years. The EBMT dataset is available in the PyMSM package at <https://github.com/hrossman/pymism>.

Appendix E. Model hyperparameters

Table 10 reports the selected hyperparameters for the MENSA model. We use Bayesian optimization (Snoek et al., 2012) to tune the hyperparameters over ten iterations in the validation set, adopting the hyperparameters leading to the lowest log-likelihood loss. Table 11 reports the selected hyperparameters for the baseline models. We configure all baseline models with sensible default hyperparameters by consulting the original work.

Hyperparameter	Synthetic	SEER	Rotterdam	MIMIC-IV	PRO-ACT	EMBT
Batch size	32	128	32	64	32	32
# Nodes per layer	[32]	[128]	[32]	[32]	[32]	[32]
Learning rate (λ)	1e-3	5e-4	1e-3	1e-3	1e-3	1e-3
Weight decay	1e-2	5e-3	1e-3	1e-3	1e-3	0.001
Dropout rate	0.25	0	0.25	0.5	0.25	0.1
Number of dists. (Ψ)	1	3	3	1	3	3

Table 10: Hyperparameters for MENSA.

Model	Parameter	Value
CoxPH	alpha	0.0001
	ties	'breslow'
	n_iter	100
	tol	1e-9
GBSA	n_estimators	100
	max_depth	1
	min_samples_split	10
	min_samples_leaf	5
	max_features	'sqrt'
	sub_sample	0.8
	random_state	0
RSF	n_estimators	100
	max_depth	1
	min_samples_split	10
	min_samples_leaf	5
	max_features	'sqrt'
	random_state	0
DeepSurv	hidden_size	100
	verbose	False
	lr	0.001
	c1	0.01
	num_epochs	1000
	dropout	0.25
	early_stop	True
patience	10	
DeepHit	num_nodes_shared	32
	num_nodes_indiv	32
	batch_norm	True
	verbose	False
	dropout	0.25
	alpha	0.2
	sigma	0.1
	batch_size	32
	lr	0.001
	weight_decay	0.01
	eta_multiplier	0.8
	epochs	1000
early_stop	True	
patience	10	
DSM	network_layers	[32]
	learning_rate	0.001
	n_iter	10000
	k	3
	batch_size	32
MTLR	verbose	False
	lr	0.001
	c1	0.01
	num_epochs	1000
	batch_size	32
	early_stop	True
patience	10	
MTLRCR	hidden_size	32
	verbose	False
	lr	1e-3
	c1	0.01
	num_epochs	1000
	dropout	0.25
	batch_size	32
	early_stop	True
patience	10	
Hierarchical	theta_layer_size	[100]
	layer_size_fine_bins	[(50, 5), (50, 5)]
	lr	0.001
	reg_constant	0.05
	n_batches	10
	batch_size	32
	backward_c_optim	False
	hierarchical_loss	True
	alpha	0.0001
	sigma	10
	use_theta	True
	use_deephit	False
	n_extra_bins	1
verbose	True	

Table 11: Hyperparameters for the baseline models.

Appendix F. Implementation details and reproducibility

All experiments were implemented and conducted in Python 3.9 using PyTorch 1.13.1, NumPy 1.24.3 and Pandas 1.5.3. Double precision (fp64) was used for tensor computations. All experiments were conducted on a single workstation with an Intel Core i9-10980XE 3.00GHz CPU, 64GB of memory, and an NVIDIA GeForce RTX 3090 GPU. CUDA 11.7 was used to perform model training on the GPU. All datasets used in this study are publicly available. Instructions on how to reproduce the results are available in the source code repository at <https://github.com/thecml/mensa>

Appendix G. Non-proportional hazards in MENSA

This section addresses how the proposed method overcomes the limitations associated with the proportional hazards assumption (Cox, 1972). We begin by reviewing how a traditional Weibull distribution adheres to the proportional hazards property and then show, intuitively, why MENSA, which uses a mixture of Weibull distributions, does not meet this assumption.

It is well-established that the Weibull distribution satisfies the proportional hazards assumption when its shape parameter, η , is independent of the covariates $\mathbf{x}^{(i)}$ (Klein and Moeschberger, 2006). The probability density function (PDF), cumulative distribution function (CDF), survival function, and hazard function for a Weibull distribution are given by:

$$\begin{aligned} f(t; \beta, \eta) &= \frac{\eta}{\beta} \left(\frac{t}{\beta}\right)^{\eta-1} \exp\left(-\left(\frac{t}{\beta}\right)^\eta\right), \\ F(t; \beta, \eta) &= \int_{\tau=0}^t f(\tau; \beta, \eta) d\tau = 1 - \exp\left(-\left(\frac{t}{\beta}\right)^\eta\right), \\ S(t; \beta, \eta) &= 1 - F(t; \beta, \eta) = \exp\left(-\left(\frac{t}{\beta}\right)^\eta\right), \\ h(t; \beta, \eta) &= \frac{f(t; \beta, \eta)}{S(t; \beta, \eta)} = \frac{\eta}{\beta} \left(\frac{t}{\beta}\right)^{\eta-1}. \end{aligned}$$

To demonstrate that the Weibull distribution satisfies the proportional hazards assumption, we parameterize the scale parameter, β , as a function of the covariates $\mathbf{x}^{(i)}$:

$$\beta(\mathbf{x}^{(i)}) = \beta_0 \exp(-\gamma^\top \mathbf{x}^{(i)}),$$

where β_0 is the baseline scale parameter, and γ is a vector of regression coefficients. Substituting $\beta(\mathbf{x}^{(i)})$ into the hazard function yields:

$$\begin{aligned} h(t; \mathbf{x}^{(i)}) &= \frac{\eta}{\beta(\mathbf{x}^{(i)})} \left(\frac{t}{\beta(\mathbf{x}^{(i)})} \right)^{\eta-1} \\ &= \frac{\eta}{\beta_0 \exp(-\gamma^\top \mathbf{x}^{(i)})} \left(\frac{t}{\beta_0 \exp(-\gamma^\top \mathbf{x}^{(i)})} \right)^{\eta-1} \\ &= \frac{\eta \exp(\gamma^\top \mathbf{x}^{(i)})}{\beta_0} \left(\frac{t \cdot \exp(\gamma^\top \mathbf{x}^{(i)})}{\beta_0} \right)^{\eta-1} \\ &= \frac{\eta}{\beta_0^\eta} t^{\eta-1} \exp(\eta \gamma^\top \mathbf{x}^{(i)}). \end{aligned}$$

We define the baseline hazard function as:

$$h_0(t) = \frac{\eta}{\beta_0^\eta} \cdot t^{\eta-1}.$$

Therefore, the hazard function can be expressed as:

$$h(t; \mathbf{x}^{(i)}) = h_0(t) \exp(\eta \gamma^\top \mathbf{x}^{(i)}). \quad (23)$$

This formulation shows that the Weibull hazard function is the product of a time-dependent baseline hazard, $h_0(t)$, and a time-independent relative hazard, $\exp(\eta \gamma^\top \mathbf{x}^{(i)})$. Hence, when the shape parameter η is constant, and only the scale parameter β varies with the covariates, the Weibull distribution satisfies the proportional hazards assumption. In contrast, both the Deep Survival Machines (DSM) (Nagpal et al., 2021) and the proposed MENSA model, which utilize a mixture of Weibull distributions, do not satisfy this assumption. This can be attributed to two main reasons:

- In DSM and MENSA, both the shape parameter η and the scale parameter β depend on the covariates $\mathbf{x}^{(i)}$. Substituting an $\mathbf{x}^{(i)}$ -dependent $\eta(\mathbf{x}^{(i)})$ into the baseline hazard definition prevents the hazard function from being expressed in a proportional hazards form, as shown in Eq. (23), thus violating the assumption.
- Since both DSM and MENSA model the survival distribution as a mixture of Weibulls, their hazard functions can be expressed through a weighted combination of individual Weibull distributions. Thus, given a weighing component, $g_\psi(\mathbf{x}^{(i)})$, the PDF (4) and CDF (5) functions, their hazard function can be described as:

$$h(t; \beta, \eta, \mathbf{x}^{(i)}) = \frac{f(t; \beta, \eta, \mathbf{x}^{(i)})}{S(t; \beta, \eta, \mathbf{x}^{(i)})} = \frac{\sum_{\psi=1}^{\Psi} g_\psi(\mathbf{x}^{(i)}) f_\psi(t; \beta_\psi(\mathbf{x}^{(i)}), \eta_\psi(\mathbf{x}^{(i)}))}{1 - \sum_{\psi=1}^{\Psi} g_\psi(\mathbf{x}^{(i)}) F_\psi(t; \beta_\psi(\mathbf{x}^{(i)}), \eta_\psi(\mathbf{x}^{(i)}))}.$$

Because the shape and scale parameters can depend on the covariates $\mathbf{x}^{(i)}$, and the model involves a mixture Weibull distributions, the resulting hazard does not adhere to a proportional hazards structure or a simple linear relationship in t or $\log(t)$. Unlike the traditional Weibull model, mixture-based approaches, such as DSM and MENSA, deviate from the proportional hazards assumption, offering greater flexibility and potentially more accurate representations of patient risk over time.